

Study on long-term warming trends in the Upper Portion of the Japan Sea Proper Water based on Argo float data

銭, 玉
九州大学大学院総合理工学府大気海洋環境システム学専攻

<https://hdl.handle.net/2324/4067777>

出版情報 : Kyushu University, 2020, 修士, 修士
バージョン :
権利関係 :

**Study on long-term warming trends in the Upper
Portion of the Japan Sea Proper Water
based on Argo float data**

QIAN YU

Supervisor: Tomoharu Senjyu

Interdisciplinary Graduate School of Engineering Sciences

Kyushu University

Contents

1. Introduction	2
2. Data and analysis method.....	9
2.1 Argo float.....	9
2.2 Argo data acquisition and screening	9
2.3 Analysis method	11
3. Results	23
3.1 Long-term trends in potential temperature in the UJSPW.....	23
3.2 Long-term trends in potential density in the UJSPW	25
4. Discussion	41
5. Conclusions	45
6. References	46
7. Acknowledgements	48

1. Introduction

The Japan Sea is a typical mid-latitude marginal sea in the Northwest Pacific Ocean (Fig. 1-1). The surface area and volume of the Japan Sea are $1.013 \times 10^6 \text{ km}^2$ and $1.69 \times 10^6 \text{ km}^3$, respectively. The mean depth of the Japan Sea is 1667 m, but the deepest portion of the sea reaches 3796 m (Senjyu 2020). The deep basin of Japan Sea consists of three major basins called the Japan Basins (JB), Tsushima Basins (TB), and the Yamato Basins (YB). Although, the Japan Sea is enclosed by the Eurasian continent, Sakhalin and Japanese Islands, it connects with the East China Sea through the Tsushima Strait, with the North Pacific through the Tsugaru Strait, and with the Okhotsk Sea through the Soya and Mamiya Straits. As all the straits are shallower than 120 m, exchange of water between the Japan Sea and the adjacent waters is limited to shallower than 200 m. Therefore, the middle and abyssal waters of the Japan Sea is completely isolated from the surrounding waters. This means that the deep water in the Japan Sea must be produced within the sea itself (Senjyu and Sudo 1993).

The vertical profiles of potential temperature (PT), salinity, dissolve oxygen (DO) concentration, and potential density referred at the sea surface (σ_θ) in the Japan Basin are shown in Fig. 1-2. Under the main thermocline, there is a distinct water mass called " the Japan Sea Proper Water (JSPW) ". The JSPW has been defined as a water mass with almost homogeneous temperature and salinity (Uda 1934); 0-1 °C and 34.06-34.07‰. The JSPW occupies more than 80% of the total volume of the Japan Sea (Yasui et al. 1967). Although the JSPW shows the very narrow temperature and salinity ranges, it can be divided into three portions: the upper portion of the JSPW (UJSPW), deep water and bottom water (Senjyu and Sudo 1993). In this study, we discuss the UJSPW that lies above approximately 1000 m.

The JSPW is formed due to the surface water cooling in the wintertime air-sea interaction in the area south of Vladivostok (Sudo 1986; Senjyu and Sudo 1993, 1994, 1996). The distribution of heat flux from sea surface to atmosphere in winter are shown in Fig. 1-3 (Kawamura and Wu 1998). The JSPW is formed in the flux center south of Vladivostok (shaded area in Fig. 1-3). The winter monsoon is blocked by the mountains on both sides of Vladivostok and can only enter the Japan Sea from the narrow valley near Vladivostok. Therefore, a strong wind area appears south of Vladivostok, which strengthens the air-sea interaction in the Japan Sea and accelerates formation of the JSPW. The monthly mean wind field on the Japan Sea in January 1997 is shown in Fig. 1-4. Wind speed on the sea south of Vladivostok is more than 9 m s^{-1} , in contrast both sides of Vladivostok are weak areas of wind.

Previous studies have been reported that the JSPW is becoming warmer year by year (Gamo 1999,2011; Minami et al. 1999). The time series of potential temperature of the JSPW at 2000 m in the Yamato and eastern Japan Basins are shown in Fig. 1-5 (Japan Meteorological Agency). Global warming has been suggested as a cause of warming trends (Gamo 1999,2011; Minami et al. 1999; Kim et al. 2001). However, whether the warming have occurred in the entire Japan Sea is still unclear, because long-term ship-board observations in the northwestern Japan Sea where the JSPW is formed were poor, especially in North Korean territory.

Recently, the amount of hydrographic data in the Japan Sea by Argo float observations has been increased. It allowed us to investigate temporal changes of the JSPW in the entire Japan Sea. In this study, we investigate the long-term variation of warming trends in the entire Japan Sea using Argo float data. In chapter 2, we introduce Argo float and Argo float data in the Japan Sea.



Fig. 1-1 Topography of the Japan Sea.
 Contour intervals are spaced at 1000 m.
 (Yoshikawa et al. 1999)

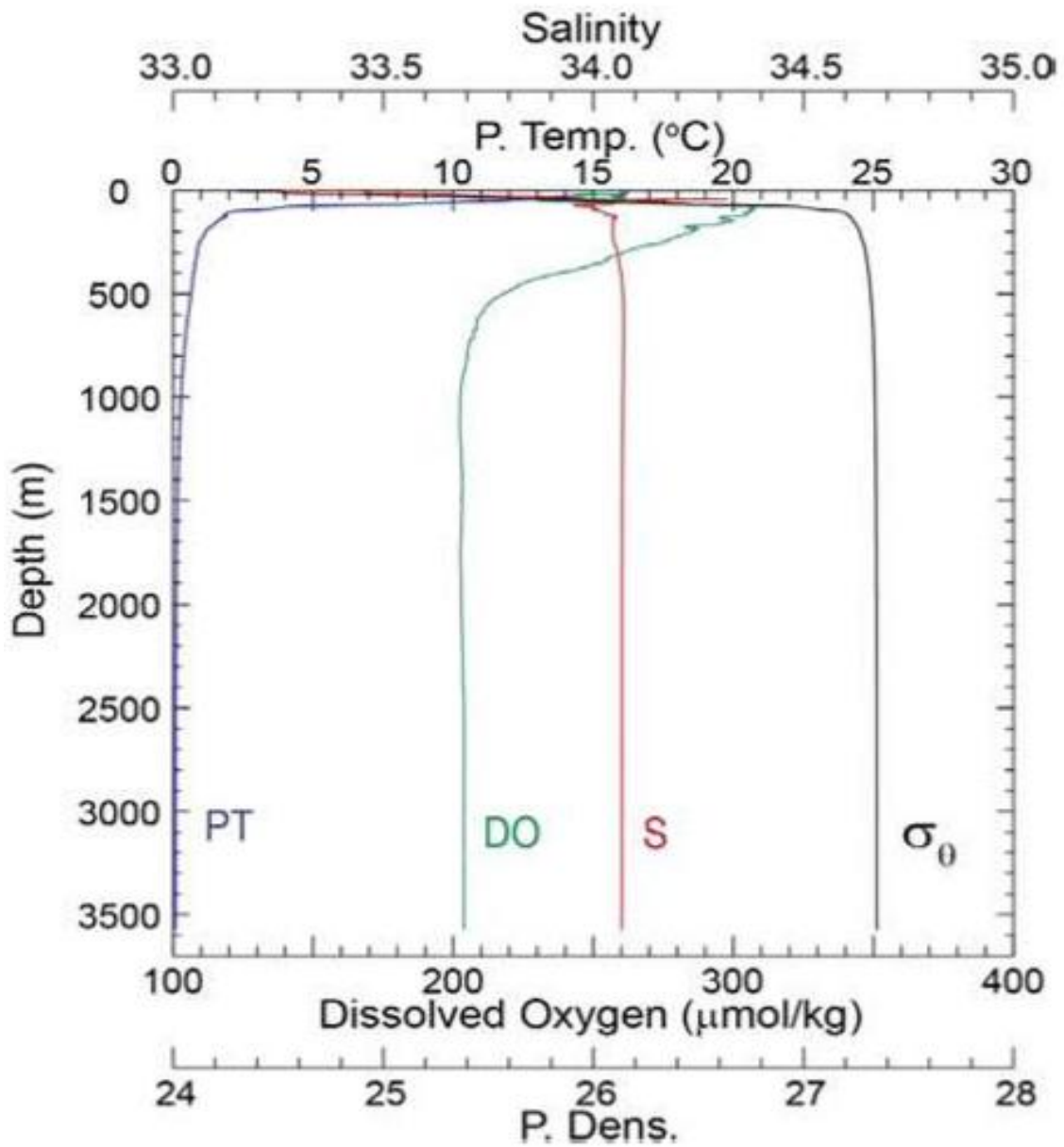


Fig. 1-2 Typical profiles of potential temperature (PT, blue), salinity (S, red), dissolved oxygen (DO, green), and potential density (σ_0 , black) in the Japan Sea, which were measured at 40° 49.34' N 137° 59.18' E in the Japan Basin on November 13, 2015 by the Japan Meteorological Agency. (Senjyu 2020)

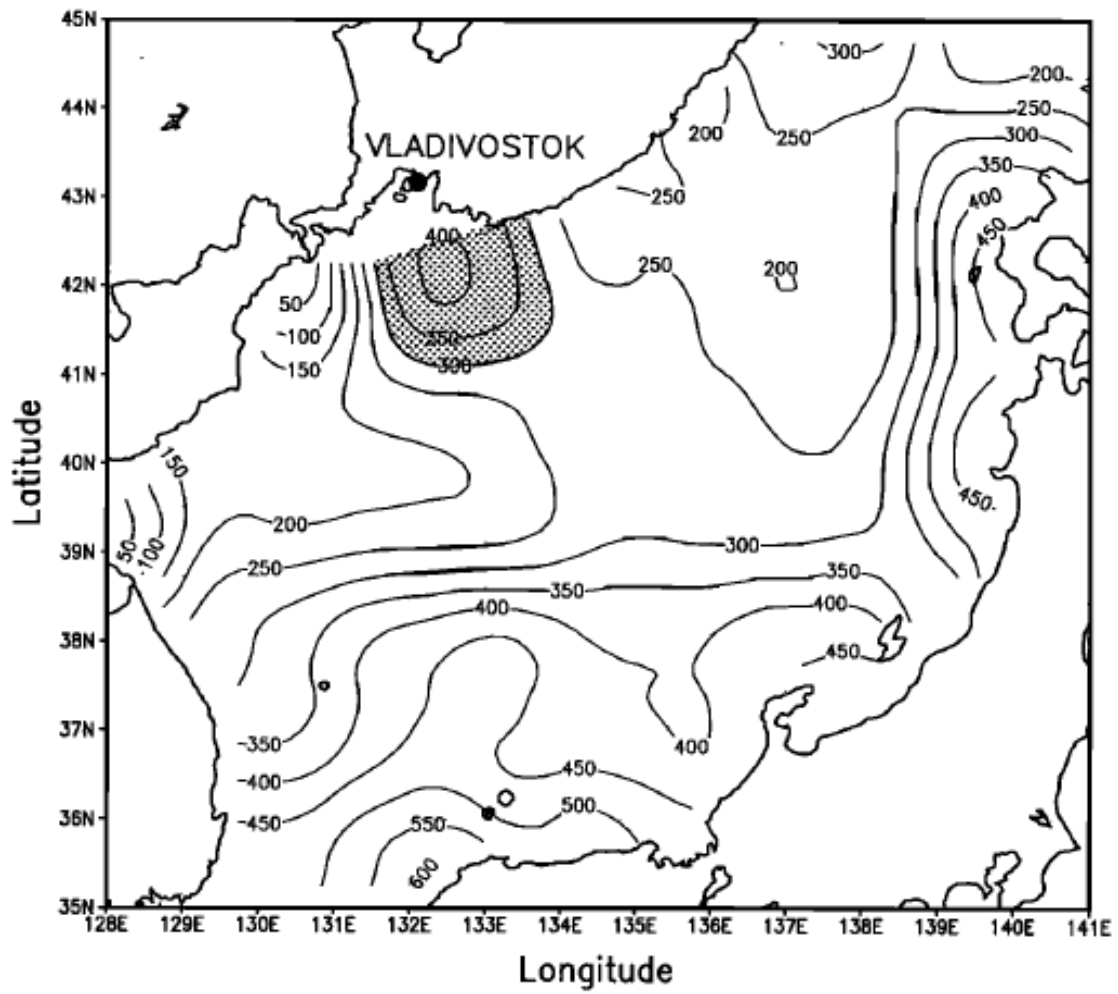


Fig. 1-3 Distribution of heat flux from the sea surface to atmosphere in the Japan Sea in January, 1997. Unit is $W m^{-2}$. The shaded area shows heat flux above $300 W m^{-2}$ (The JSPW formation area). (Kawamura and Wu 1998)

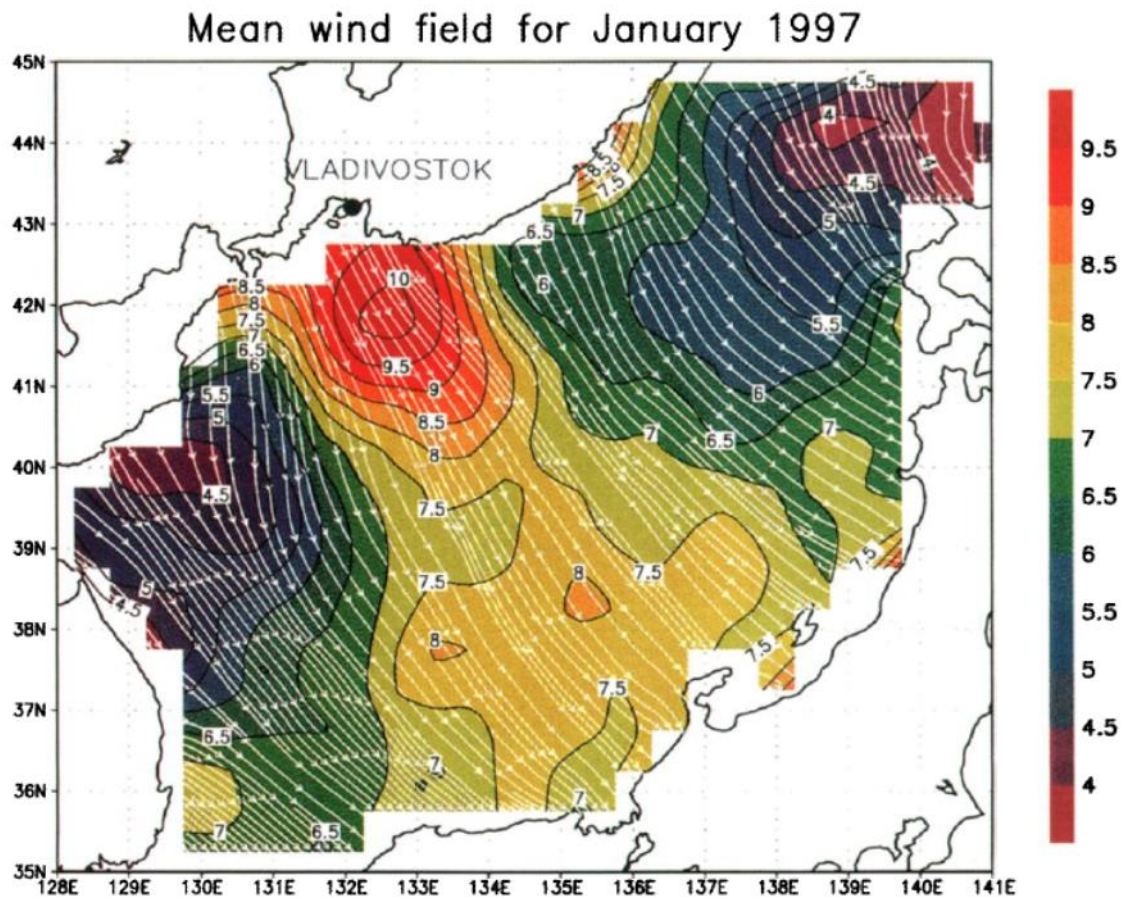


Fig. 1-4 Monthly mean wind field over the Japan Sea in January 1997, in meters per second. Wind speeds are illustrated by color, and white streamlines are superimposed with arrows. The area off Vladivostok with a wind speed of $>9 \text{ m s}^{-1}$ is shown in red. (Kawamura and Wu 1998)

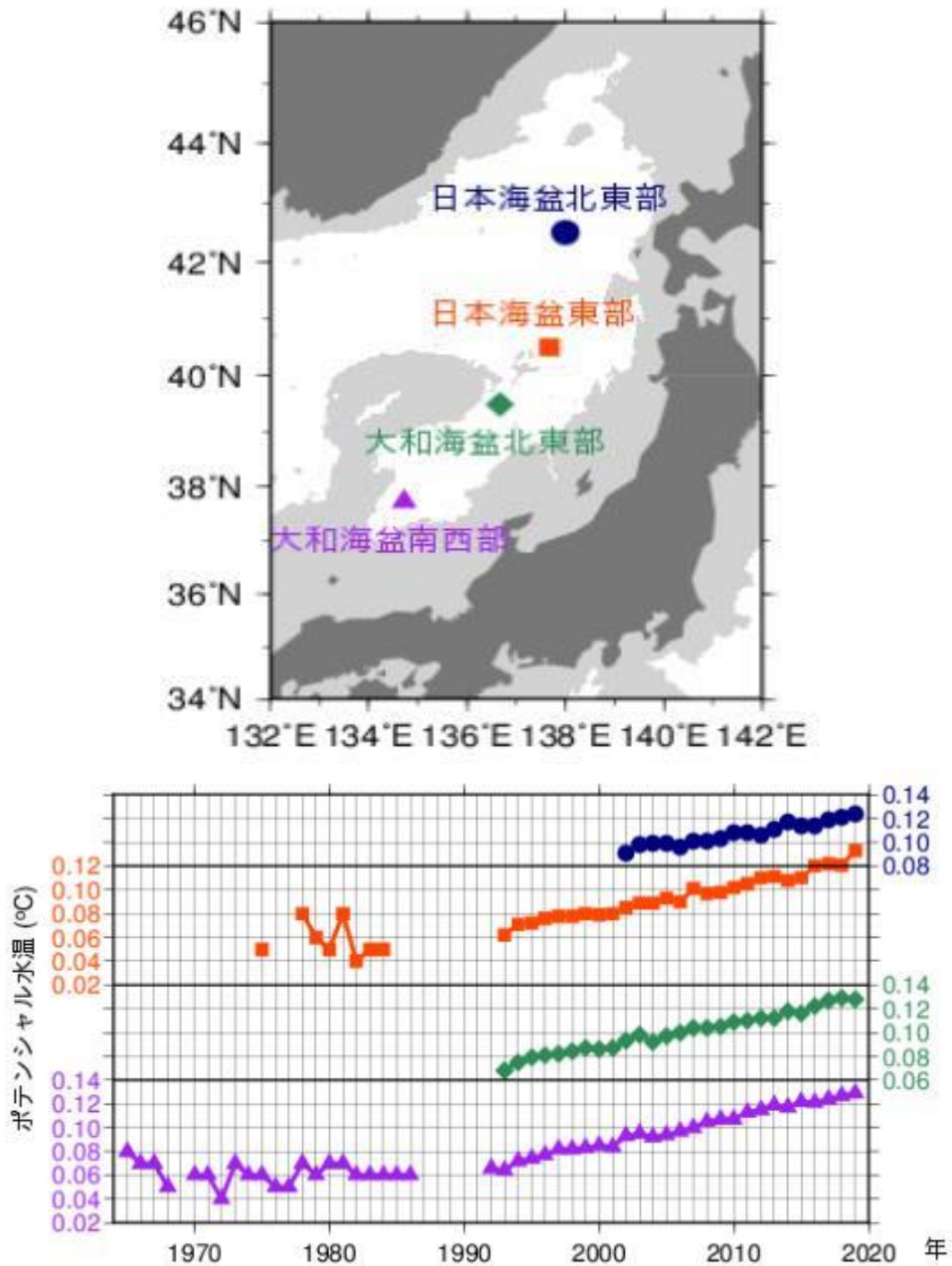


Fig. 1-5 Location of observation stations by the Japan Meteorological Agency in the Yamato and Japan Basins (upper) and the time series of potential temperature at 2000 m at each station (lower).
 (Japan Meteorological Agency, https://www.data.jma.go.jp/gmd/kaiyou/shindan/e_2/maizuru_koyusui/maizuru_koyusui.html)

2. Data and analysis method

2.1 Argo float

Argo floats are robots that collect oceanographic data from the sea surface to 2000 m (Fig. 2-1). They surface every certain period (about ten days) and send data of temperature and salinity to a satellite. Then the float returns to its original density and drift until the next cycle. Floats are designed to make about 150 cycles for 3-4 years (Japan Agency for Marine-Earth Science and Technology, JAMSTEC).

Deployments of Argo began in 2000 and continue today at the rate of about 800 per year involving more than 50 research and operation agencies (http://www.argo.ucsd.edu/About_Argo.html). Nowadays, Argo floats are widely distributed all over the world ocean and have already become the main component of the ocean observing system. Argo data is freely available from two global data servers in France and USA.

2.2 Argo data acquisition and screening

In the Japan Sea, there are little Argo floats data deeper than 1000 m, because most of the data is concentrated upper 700 m due to the shallower depths than the Northwest Pacific Ocean. Therefore, in this study, deep water and bottom water under the UJSPW cannot be studied.

One of the characteristics of the Argo plan is that the profile data from Argo floats are released immediately (http://www.jamstec.go.jp/ARGO/argo_web/argo/page_id=100&lang=ja). However, the real-time Quality Controlled process (rQC) in the Argo plans is simple and is not suitable for research. On the other hand, the delayed quality controlled process guarantees the accuracy of the research, but it takes half a year to publish, it is

not suitable for immediate monitoring of sea conditions. To solve this problem, JAMSTEC provides the Advanced Quality Controlled Argo data (AQC Argo Data) which were automatically advanced quality controlled process than rQC to the Argo profile. In this study, the AQC Argo Data in the Japan Sea during the period 2001-2019 were analyzed.

Since the AQC Argo data included insufficient accuracy data to study, particularly in salinity in the JSPW, we made further quality control to the AQC Argo datasets. Firstly, we only selected the vertical profiles that were deeper than 500 m (Fig. 2-2). Secondly, we screened the selected vertical profiles of salinity: ① If the deepest salinity measurement in a profile was between 34.06-34.07 ‰, the profile data were used normally; ② If the deepest salinity measurement in a profile was higher than 34.07 ‰ and lower than 34.1 ‰, we added the difference between 34.068 ‰ and the deepest salinity to the all profile of salinity; ③ If the deepest salinity measurement in a profile was lower than 34.06 and higher than 34.02 ‰, we added the difference between 34.068 ‰ and deepest salinity to the all profile of salinity; ④ If the deepest salinity measurement in a profile was higher than 34.1 ‰ or lower than 34.02 ‰, we did not use this profile (Fig. 2-3).

The distribution of Argo floats in 2001-2019 were shown in Fig. 2-4. In 2001, there were no Argo floats in the north and only few Argo floats distributed in the southwest of the Japan Sea (Fig. 2-4a). Since then, the number of Argo floats have increased year by year. By 2005, there were many Argo floats in the southern Japan Sea, but few Argo floats were distributed in the north (Fig. 2-4e). After 2009, Argo floats were distributed in most areas of the Japan Sea (Fig. 2-4i-s). The distribution of all the data in 2001-2019 (Fig. 2-4t) shows that the entire Japan Sea was occupied by Argo floats data.

2.3 Analysis method

After the screening of the Argo profiles, we classified the Argo data into four regions: the western Japan Basin (JW), eastern Japan Basin (JE), Tsushima Basin (TB), and Yamato Basin (YB) for each year (Table 2-1 and Fig. 2-4). The number of Argo floats in the four regions in 2001-2019 and its time variations are shown in Table 2-2 and Fig. 2-5. From 2001 to 2003, there was no Argo float in JW, JE, and YB. However, Argo floats in YB, JE, and JW increased since 2004, 2005, and 2006 respectively. Since 2006, the number of Argo floats in the four regions have been more than 20 continuously. The number of Argo floats in TB is more than that in YB, JE, and JW before 2009, but YB has the largest number of Argo floats since 2011.

All profiles were interpolated every 10 dbar using the Akima Spline method (Akima, 1970). From pressure, temperature and salinity of each interpolated profile, the potential temperature and potential density for each profile were calculated. Then, mean potential temperature, salinity and potential density in each year (2001-2019), depth (400, 500, 600, 650, and 700 m), and region (JW, JE, TB, and YB) were calculated. In this calculation, we further screened the profiles: if the potential temperature at 400 m was higher than 1.0 °C, this profile was removed. This is because one of the characteristics of the UJSPW is lower than 1.0 °C. The higher potential temperature was likely to be affected by the warm eddies.

For the calculation of mean potential temperature and potential density, we used more than three data. The number of Argo profiles at 400, 500, 600, 650, and 700 m in the four regions during 2001-2019 are shown in Table 2-3. The red number means that the profiles were less than three, we did not calculate the mean values.

Table 2-1 Location of analyzing areas

JW	40.0-42.0N	131.0-133.0E
JE	41.0-43.0N	136.5-138.5E
TB	35.0-37.0N	130.0-133.0E
YB	36.0-39.0N	134.5-137.0E

Table 2-2 The number of Argo floats in the four analyzing areas during 2001-2019

	JW	JE	TB	YB	total
2001	0	0	25	0	43
2002	0	0	102	1	211
2003	0	0	171	1	341
2004	0	0	148	52	603
2005	0	34	197	58	810
2006	32	15	294	43	1045
2007	10	32	378	15	1112
2008	11	36	204	79	1133
2009	46	38	211	204	1445
2010	35	109	96	94	1510
2011	19	54	31	84	1026
2012	13	26	56	200	896
2013	13	33	22	121	803
2014	12	20	65	103	806
2015	5	55	48	63	677
2016	11	27	10	33	472
2017	90	113	92	127	1439
2018	67	98	53	146	1007
2019	22	49	30	62	749

Table 2-3 The number of Argo profiles at 400, 500, 600, 650, and 700 m in the four regions during 2001-2019

JW					
	n400	n500	n600	n650	n700
2001	0	0	0	0	0
2002	0	0	0	0	0
2003	0	0	0	0	0
2004	0	0	0	0	0
2005	0	0	0	0	0
2006	31	31	31	21	1
2007	10	10	9	5	0
2008	11	11	9	4	1
2009	45	45	43	37	0
2010	26	26	26	24	11
2011	18	18	18	16	0
2012	13	13	12	9	2
2013	13	13	13	11	6
2014	11	11	11	9	0
2015	5	5	5	5	5
2016	5	5	5	3	2
2017	81	81	81	79	65
2018	67	67	67	67	57
2019	19	19	19	19	17

JE					
	n400	n500	n600	n650	n700
2001	0	0	0	0	0
2002	0	0	0	0	0
2003	0	0	0	0	0
2004	6	6	6	2	0
2005	21	21	21	17	0
2006	9	9	9	8	0
2007	20	20	18	15	0
2008	30	30	26	21	0
2009	38	38	36	19	6
2010	106	106	106	103	90
2011	54	54	54	45	0
2012	26	26	26	14	4
2013	27	27	27	19	15
2014	20	20	20	19	18
2015	55	55	55	55	45
2016	25	25	25	25	9
2017	102	102	101	91	69
2018	95	95	89	83	79
2019	49	49	45	44	44

Table 2-3 (continued)

TB						YB					
	n400	n500	n600	n650	n700		n400	n500	n600	n650	n700
2001	25	25	24	20	1	2001	0	0	0	0	0
2002	102	102	101	76	6	2002	0	0	0	0	0
2003	171	171	168	138	28	2003	1	1	1	1	0
2004	145	145	139	102	10	2004	51	51	50	45	0
2005	187	187	184	132	20	2005	54	54	54	37	3
2006	271	271	264	205	47	2006	42	42	39	24	0
2007	372	372	347	260	81	2007	10	10	10	9	2
2008	202	202	189	148	17	2008	58	58	53	43	3
2009	211	211	199	148	14	2009	175	175	162	138	81
2010	95	95	84	63	11	2010	82	82	80	65	29
2011	31	31	31	30	24	2011	74	74	74	51	20
2012	55	55	55	48	28	2012	151	151	143	108	37
2013	20	20	20	20	14	2013	103	103	96	69	35
2014	60	60	60	55	34	2014	91	91	87	85	57
2015	46	46	45	45	32	2015	45	45	43	35	15
2016	8	8	8	8	8	2016	32	32	32	25	21
2017	89	89	89	88	87	2017	117	117	114	112	108
2018	48	48	48	48	48	2018	130	130	128	125	119
2019	22	22	22	22	22	2019	59	59	57	55	54

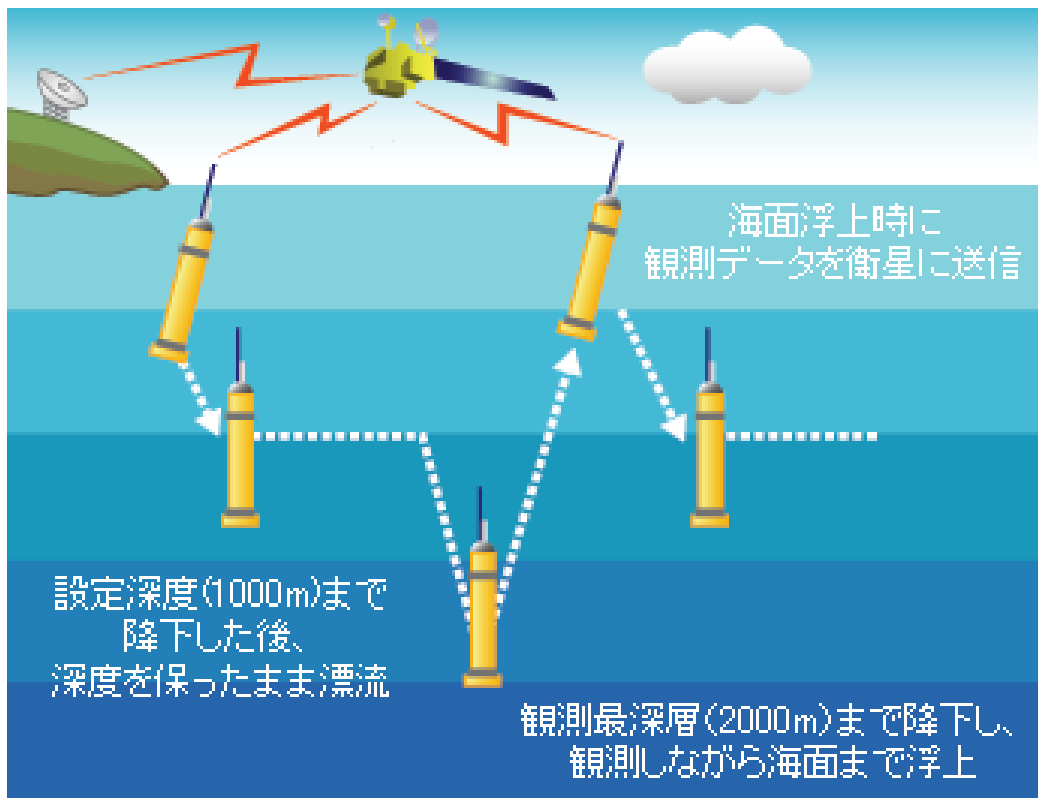


Fig. 2-1 Conceptual diagram of Argo float operation cycle.
 (JAMSTEC, http://www.jamstec.go.jp/J-ARGO/overview/overview_3.html)

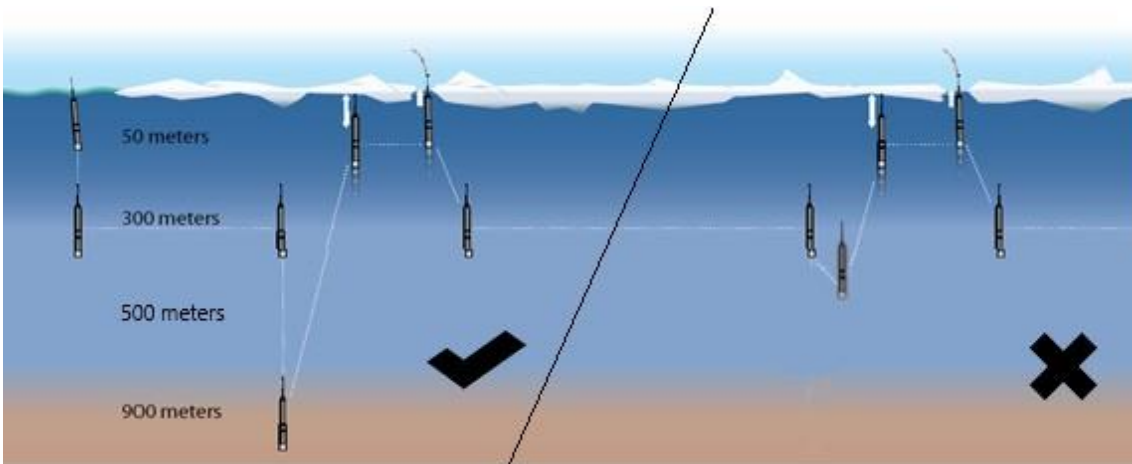


Fig. 2-2 Example of Argo float operation cycle. On the left, Argo float operated deeper than 500 m. In this case, the vertical profile was used in this study. On the right, Argo float operated shallower than 500 m. In this case, the vertical profile was not used in this study.

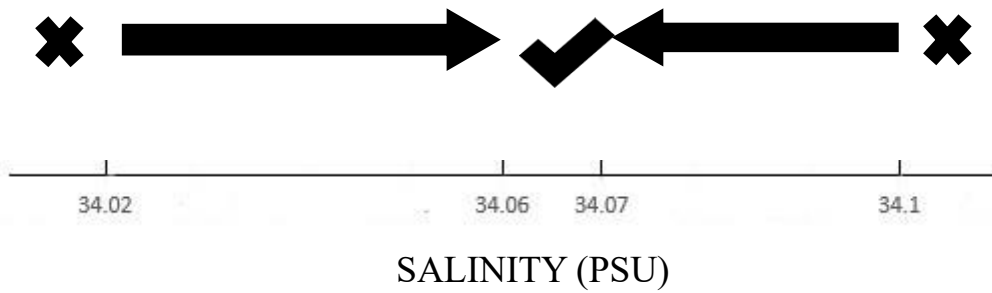


Fig. 2-3 Salinity screening range diagram.

The symbol “×” indicates that the profile data were not used; “→” and “←” indicate that the data were auxiliary corrected; “√” indicate that the profile data were used.

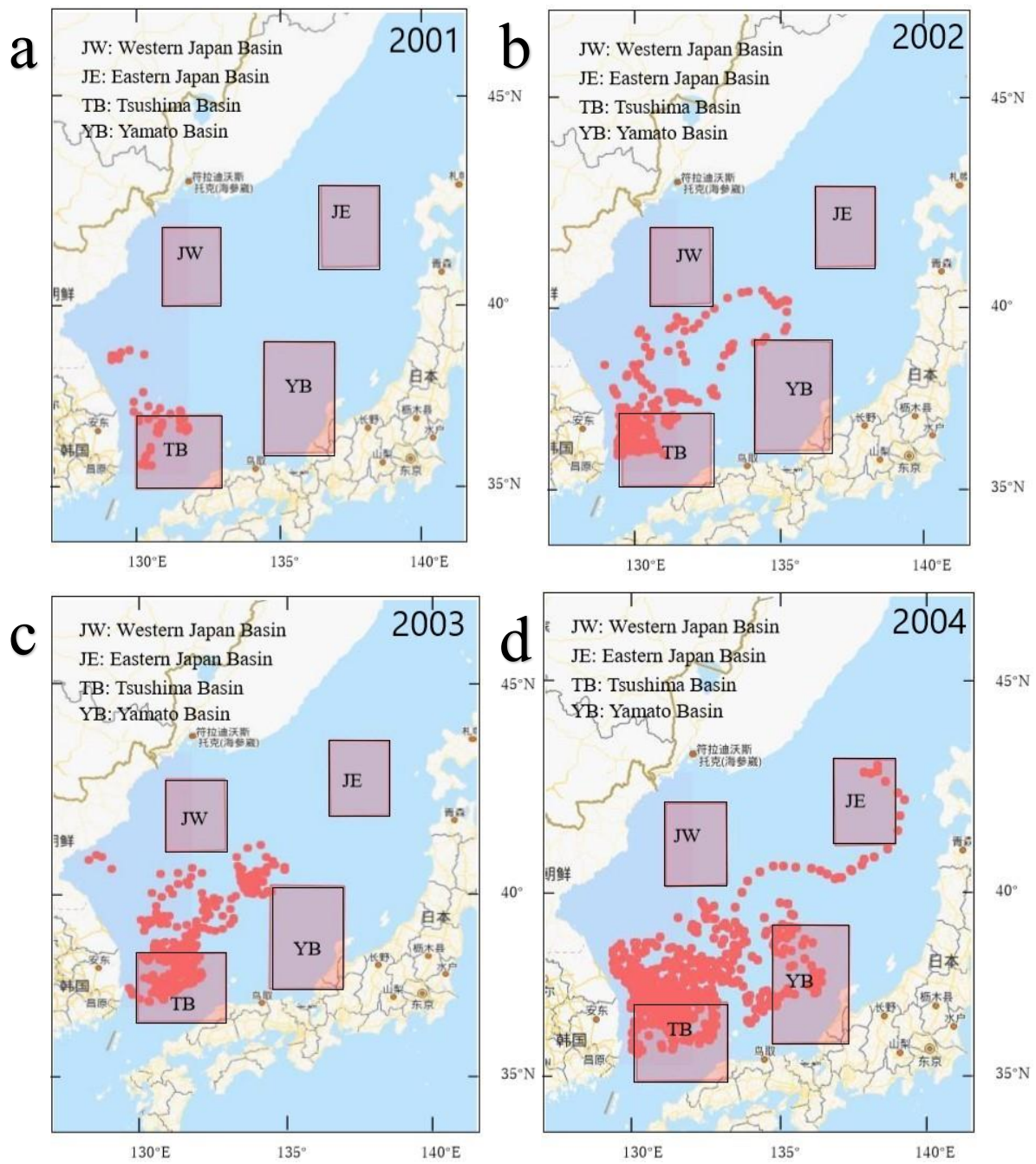


Fig. 2-4 Location of Argo floats (red dots) in each year during 2001-2019 and four analyzing areas (red squares).

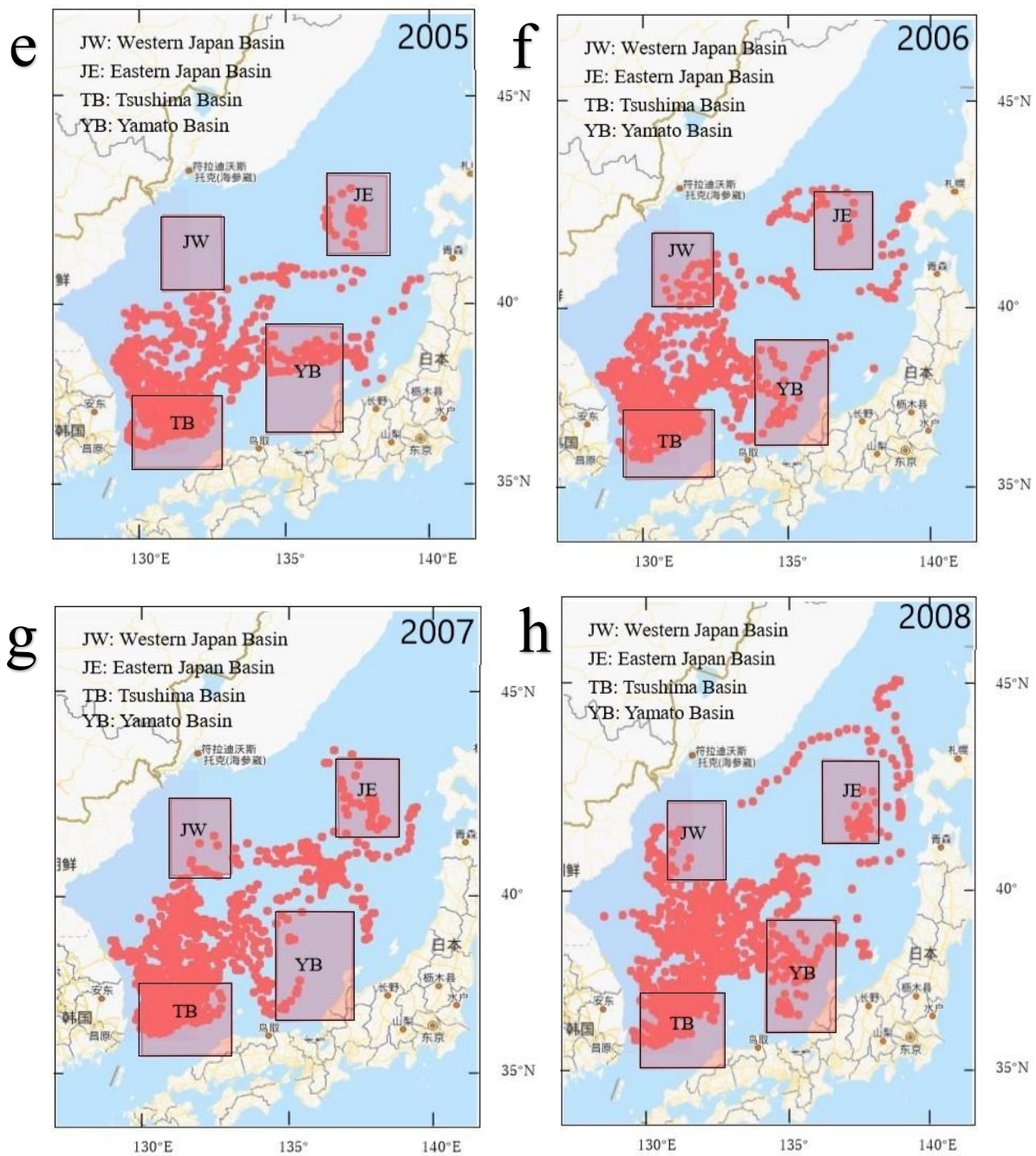


Fig. 2-4 (continued)

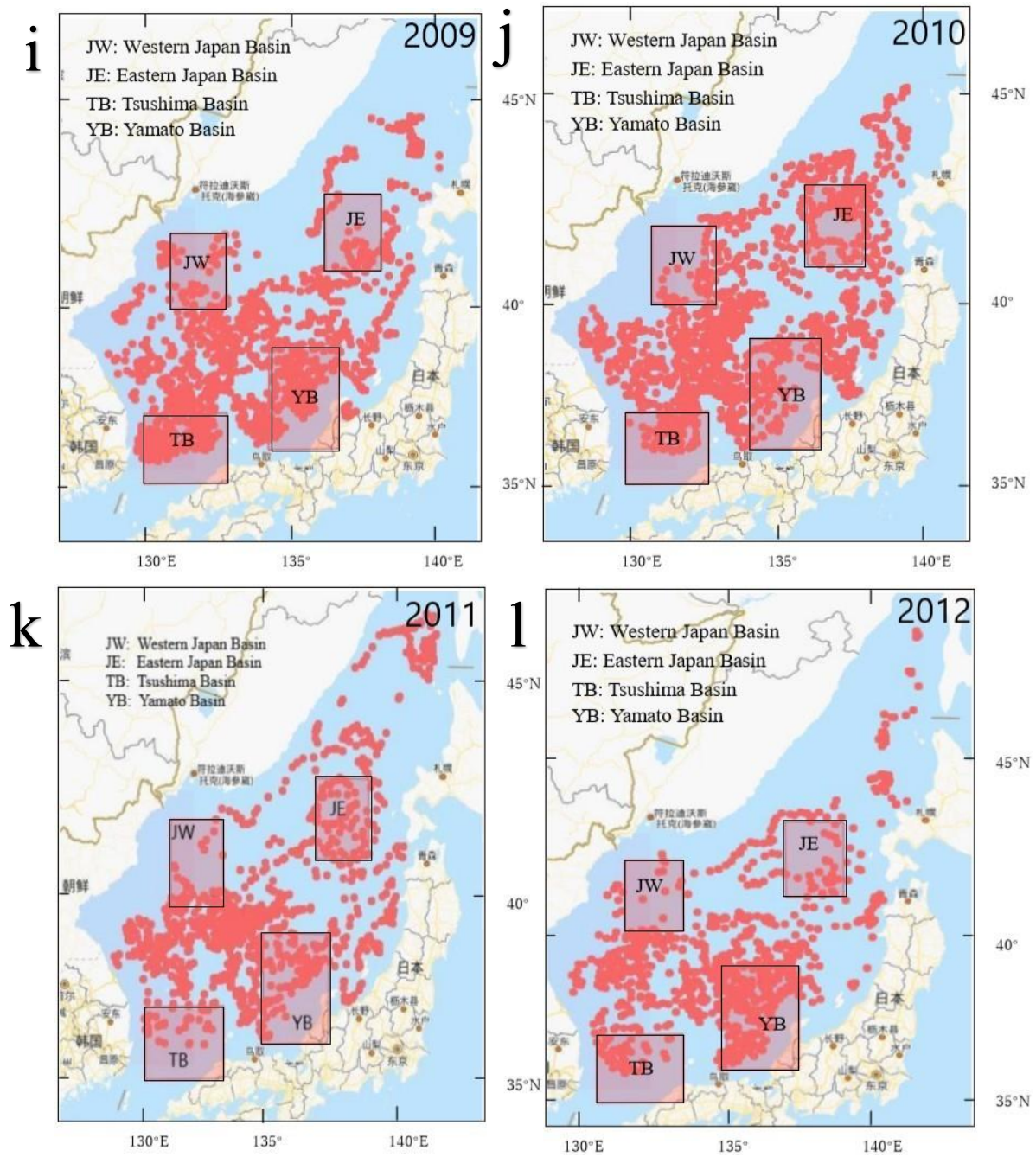


Fig. 2-4 (continued)

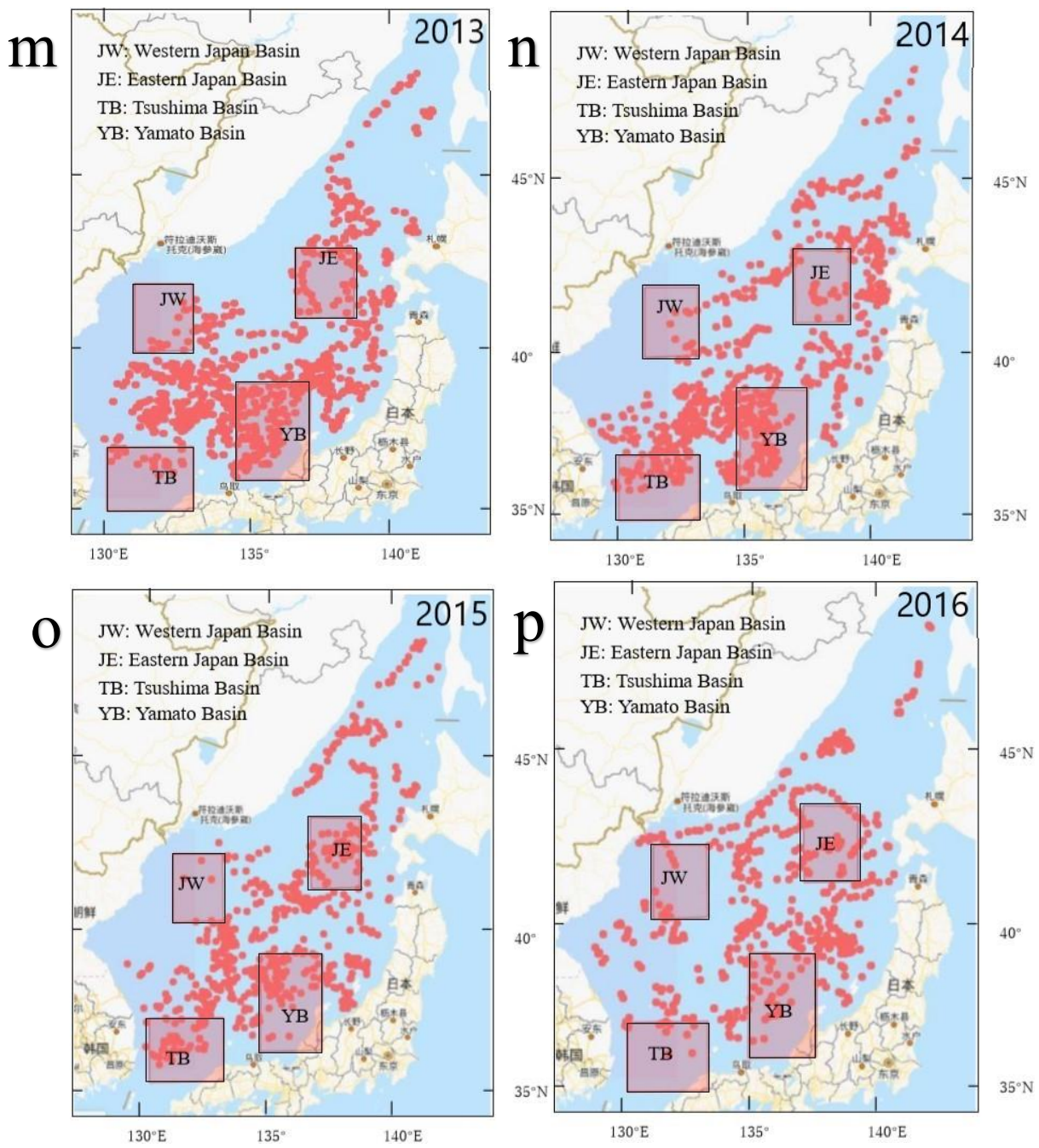


Fig. 2-4 (continued)

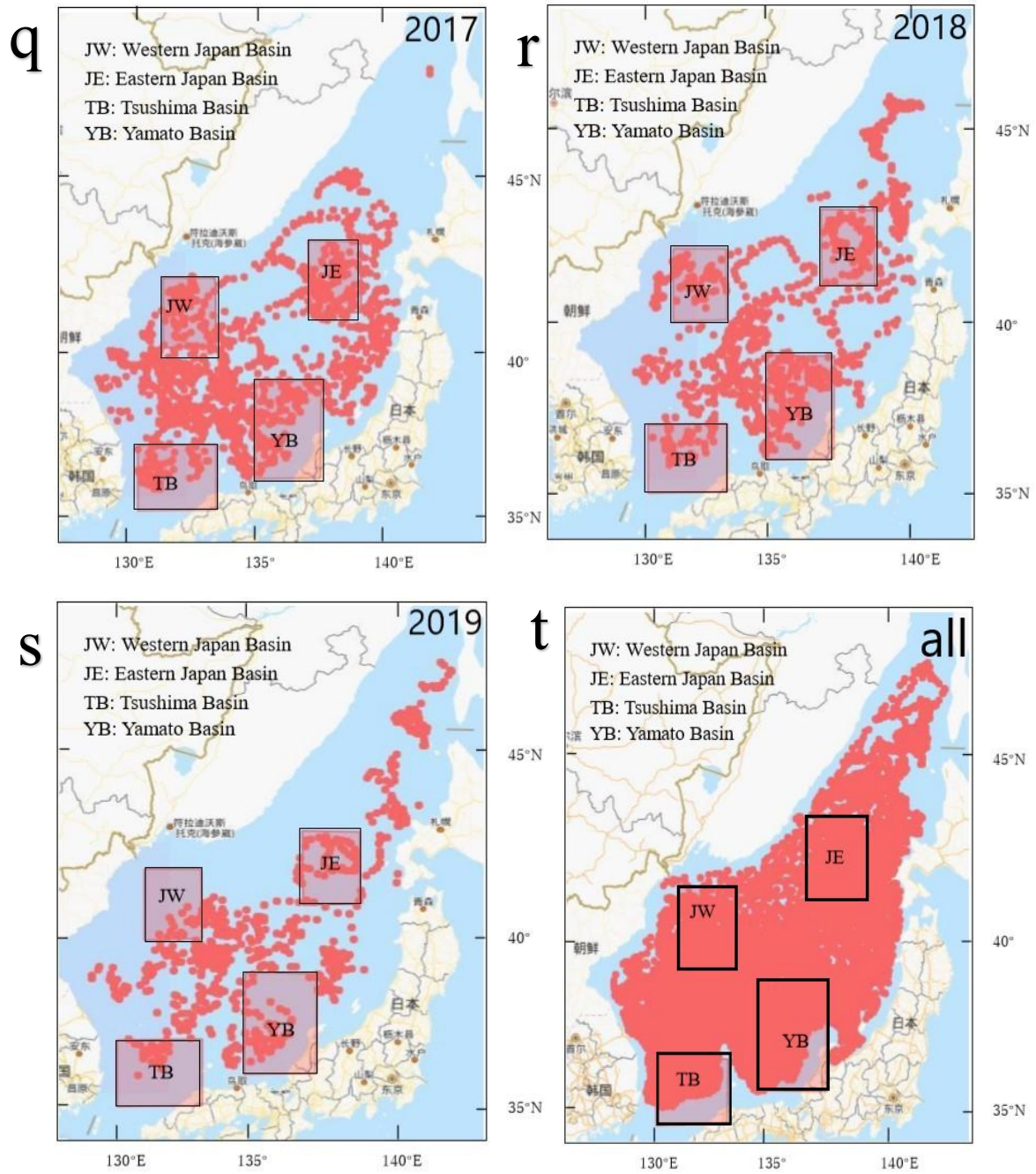


Fig. 2-4 (continued)

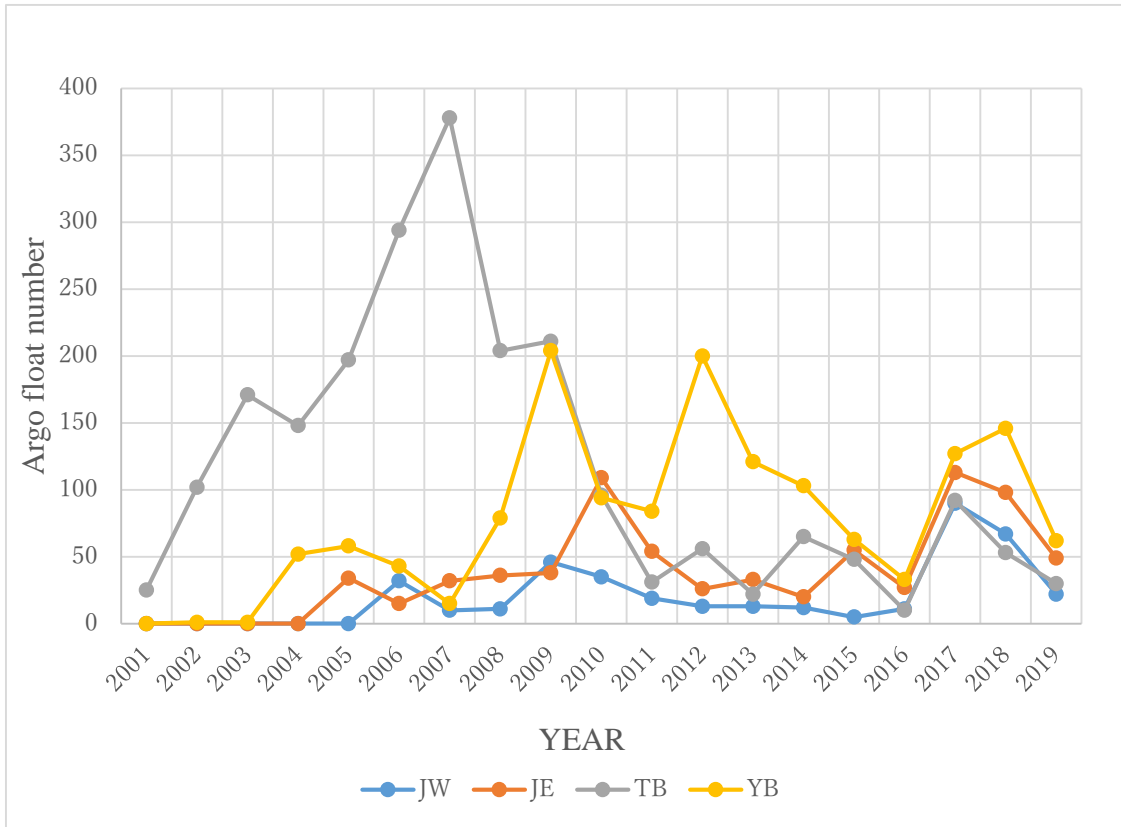


Fig.2.5 Time series of the number of Argo floats in the four analyzing areas.

3. Results

3.1 Long-term trends in potential temperature in the UJSPW

Time-series and warming rates of potential temperature at 400, 500, 600, 650, and 700 m in the four regions are shown in Fig. 3-1 to Fig. 3-5, respectively. The warming rates are calculated using least square method. The gradual warming of water over the recent decades have been recognized throughout the water column from 400 to 700 m in all the four regions, except for the case of JE at 400 m. Although almost all the regions were in the warming trends, the warming rates were not homogeneous. At the depth of 400 m, JW, TB, and YB shows warming trends at +0.0027, +0.0128, and +0.0082 °C/year respectively, although JE shows a negative rate at -0.0010 °C/year. At the depth of 500 m, the warming rates in JW, JE, TB, and YB are +0.0049, +0.0022, +0.0121, and +0.0097 °C/year, respectively. At the depth of 600 m, the warming rates in JW, JE, TB, and YB are +0.0056, +0.0030, +0.0112, and +0.0093 °C/year, respectively. At the depth of 650 m, the warming rates in JW, JE, TB, and YB are +0.0055, +0.0022, +0.0103, and +0.0088 °C/year, respectively. At the depth of 700 m, the warming rates in JW, JE, TB, and YB are +0.0077, +0.0050, +0.0103, and +0.0074 °C/year, respectively (Table 3-1). An interesting point is that the warming rates in TB and YB in the southern Japan Sea were higher than those in JW and JE in the northern sea by 2-4 times at all the depths.

Although warming trends are recognized in the most of regions, considerable inter-annual variation is found in some areas, compared with the linear trend (for example, at 400 m in JW and JE). Therefore, to check the statistical significance of the linear trends, we carried out the t-test (Student's t-test) (Table 3-1). The t-test was carried out by the following steps: firstly, the correlation coefficients r between the year and corresponding mean potential temperatures were calculated. Secondly, the statistic $T(r, 0)$ was

calculated as:

$$T(r, 0) = \frac{r\sqrt{N-2}}{\sqrt{1-r^2}} \quad (1),$$

where N denote the number of data. Thirdly, we compared the statistic $T(r, 0)$ with the t-distribution table at degree of freedom $N-2$ to determine the significance level. The test results are shown in Table 3-1, significance levels at 99%, 95% and less than 95% are shown by red, blue and black numbers, respectively. TB and YB have higher significance than that of JW and JE. The negative rate in JE at 400 m are not statistically significant.

To see the structure of potential temperature field, the time variation of profile is shown in Fig. 3-6. We confirmed following features: ① Potential temperature in the four regions increased gradually year by year throughout depths from 400 to 700 m. ② In JE, the potential temperature increase during 2006-2012 (6 years) is more than that in 2012-2018 (6 years) in the range 400-600 m; the potential temperature increase during 2012-2018 (6 years) is more than that in 2006-2012 (6 years) in the range 600-700 m. ③ In TB, the potential temperature increase during 2012-2018 (6 years) is more than that in 2006-2012 (6 years) in the range 400-700 m. ④ In YB, the potential temperature increase during 2006-2012 (6 years) is more than that in 2012-2018 (6 years) in the range 400-700 m. ⑤ In JW, potential temperature variations are complicated. ⑥ In the same years (2006-2012), YB has the most temperature increase, followed by JE and TB. ⑦ In the same period (2012-2018), TB has the largest temperature increase, followed by YB and JE.

3.2 Long-term trends in potential density in the UJSPW

Time-series and changing rates of potential density at 400, 500, 600, 650, and 700 m in the four regions are shown in Fig. 3-7 to Fig. 3-11, respectively. Overall potential density shows decrease trends. We obtained the following changing rates using least square method: at the depth of 400 m, the changing rates in JW, JE, TB, and YB are -0.0015, -0.0008, -0.0016, and -0.0012 kg/m³/year, respectively. At the depth of 500 m, the changing rates in JW, JE, TB, and YB are -0.0010, -0.0005, -0.0011, and -0.0009 kg/m³/year, respectively. At the depth of 600 m, the changing rates in JW, JE, TB, and YB are -0.0006, -0.0003, -0.0007, and -0.0006 kg/m³/year, respectively. At the depth of 650 m, the changing rates in JW, JE, TB, and YB are -0.0005, -0.0001, -0.0006, and -0.0005 kg/m³/year, respectively. At the depth of 700 m, the changing rates in JW, JE, TB, and YB are -0.0005, -0.0005, -0.0006, and -0.0004 kg/m³/year, respectively (Table 3-2). In accordance with the warming trends in potential temperature, gradual decrease of potential density over the recent decades are recognized throughout the water column from 400 to 700 m in the four regions.

We carried out the t-test (Student's t-test) to examine the statistical significance of each trend (Table 3-2). Negative rates in all the four regions are statistically significant. TB and YB have higher significance than that of JW and JE, especially in 600-700 m.

To see the structure of potential density field, the time variation of profile is shown in Fig. 3-12. We confirmed following features: ① Potential density in the four regions decreased gradually year by year in throughout depths from 400 to 700 m. ② In JW, the potential density decrease during 2012-2018 (6 years) is more than that in 2006-2012 (6 years) in the range 400-650 m; potential density decreased and increased during 2006-2012 (6 years) and 2012-2018 (6 years), respectively at 700 m. ③ In JE, the potential

density decrease during 2012-2018 (6 years) is more than that in 2006-2012 (6 years) in the range 400-700 m. ④ In TB, the potential density decrease during 2012-2018 (6 years) is more than that in 2006-2012 (6 years) in the range 400-650 m; the potential density decrease during 2006-2012 (6 years) is more than that in 2012-2018 (6 years) at 700 m. ⑤ In YB, the potential density decrease during 2006-2012 (6 years) is more than that in 2012- 2018 (6 years) in the range 400-700 m. ⑥ In the same period (2006-2012), YB showed the most potential density decrease, followed by JW, JE and TB. ⑦ In the same period (2012-2018), JE and TB have the largest potential density decrease, followed by JW and YB.

Table 3-1 Warming rates at 99% (red number), 95% (blue number), and less than 95% (black number) significance levels in each region at each depth

Depth(m)	JW	JE	TB	YB
400	+0.0027	-0.0010	+0.0128	+0.0082
500	+0.0049	+0.0022	+0.0121	+0.0097
600	+0.0056	+0.0030	+0.0112	+0.0093
650	+0.0055	+0.0022	+0.0103	+0.0088
700	+0.0077	+0.0050	+0.0103	+0.0074

Table 3-2 Changing rates of potential density at 99% (red number), 95% (blue number), and less than 95% (black number) significance levels in each region at each depth

Depth(m)	JW	JE	TB	YB
400	-0.0015	-0.0008	-0.0016	-0.0012
500	-0.0010	-0.0005	-0.0011	-0.0009
600	-0.0006	-0.0003	-0.0007	-0.0006
650	-0.0005	-0.0001	-0.0006	-0.0005
700	-0.0005	-0.0005	-0.0006	-0.0004

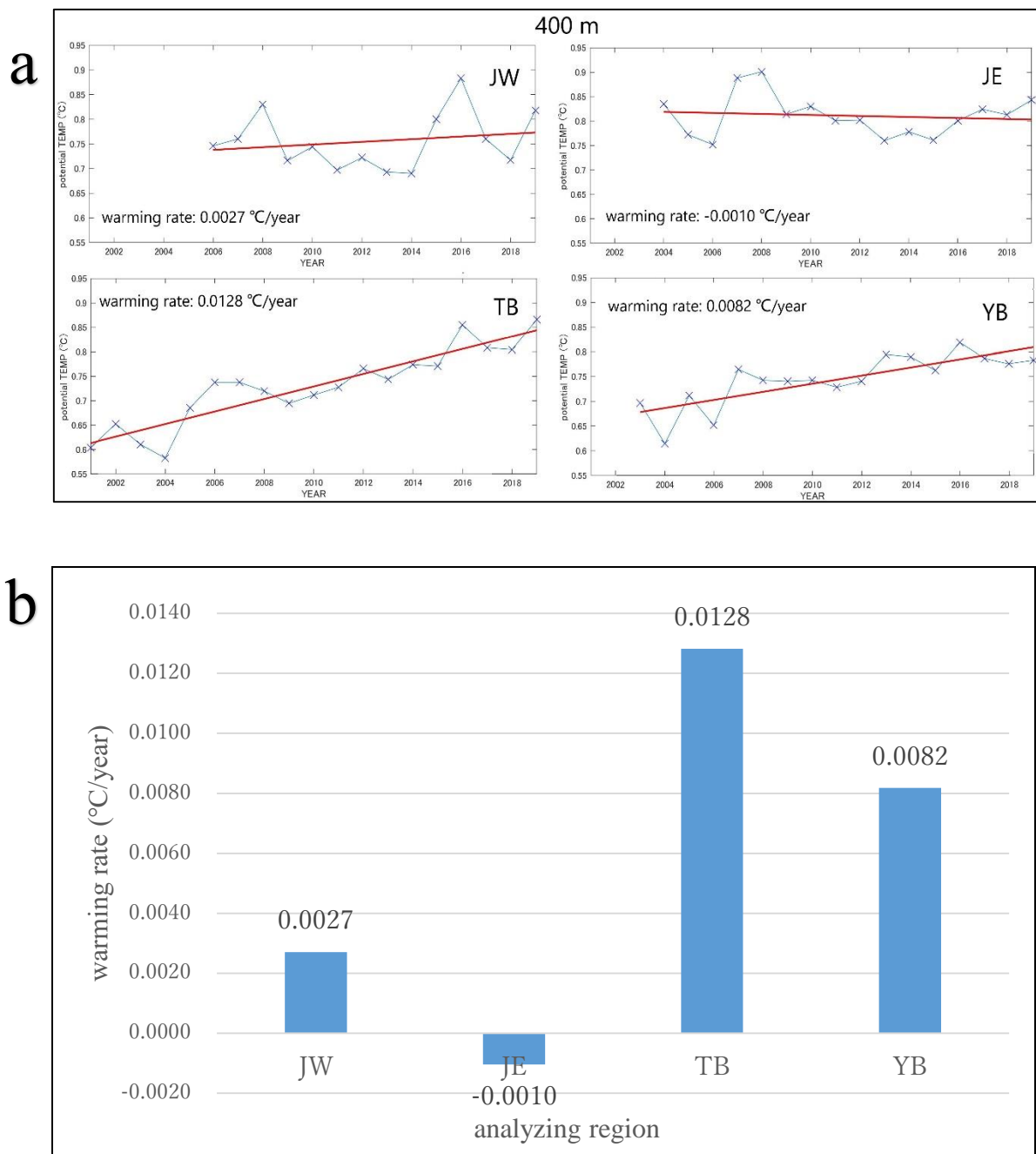


Fig. 3-1 Time-series of potential temperature at 400 m in each region (a). Blue dots denote the annual means and red lines indicate the linear trends. Warming rate of potential temperature in each region at 400 m (b).

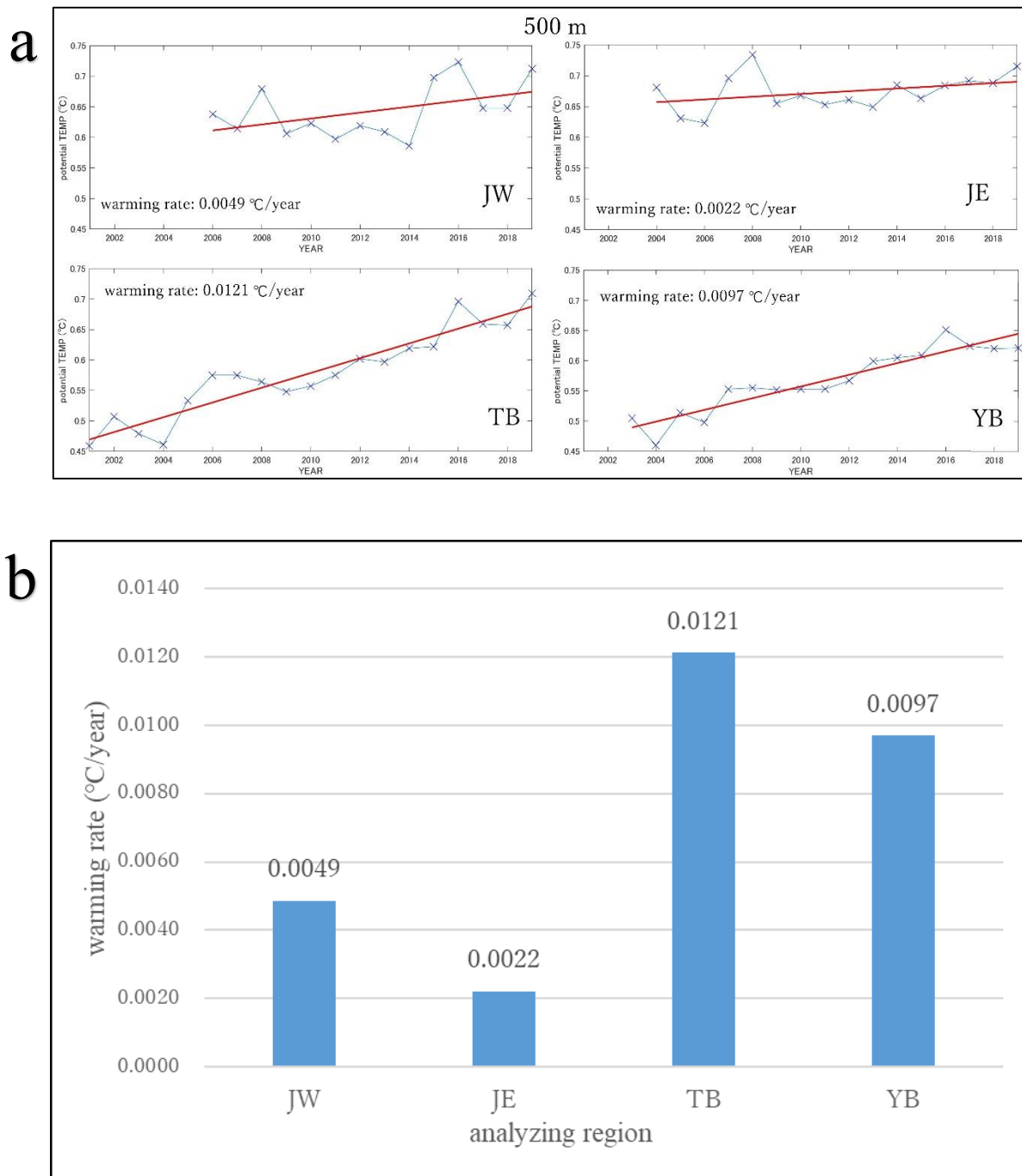


Fig. 3-2 Time-series of potential temperature at 500 m in each region (a). Blue dots denote the annual means and red lines indicate the linear trends. Warming rate of potential temperature in each region at 500 m (b).

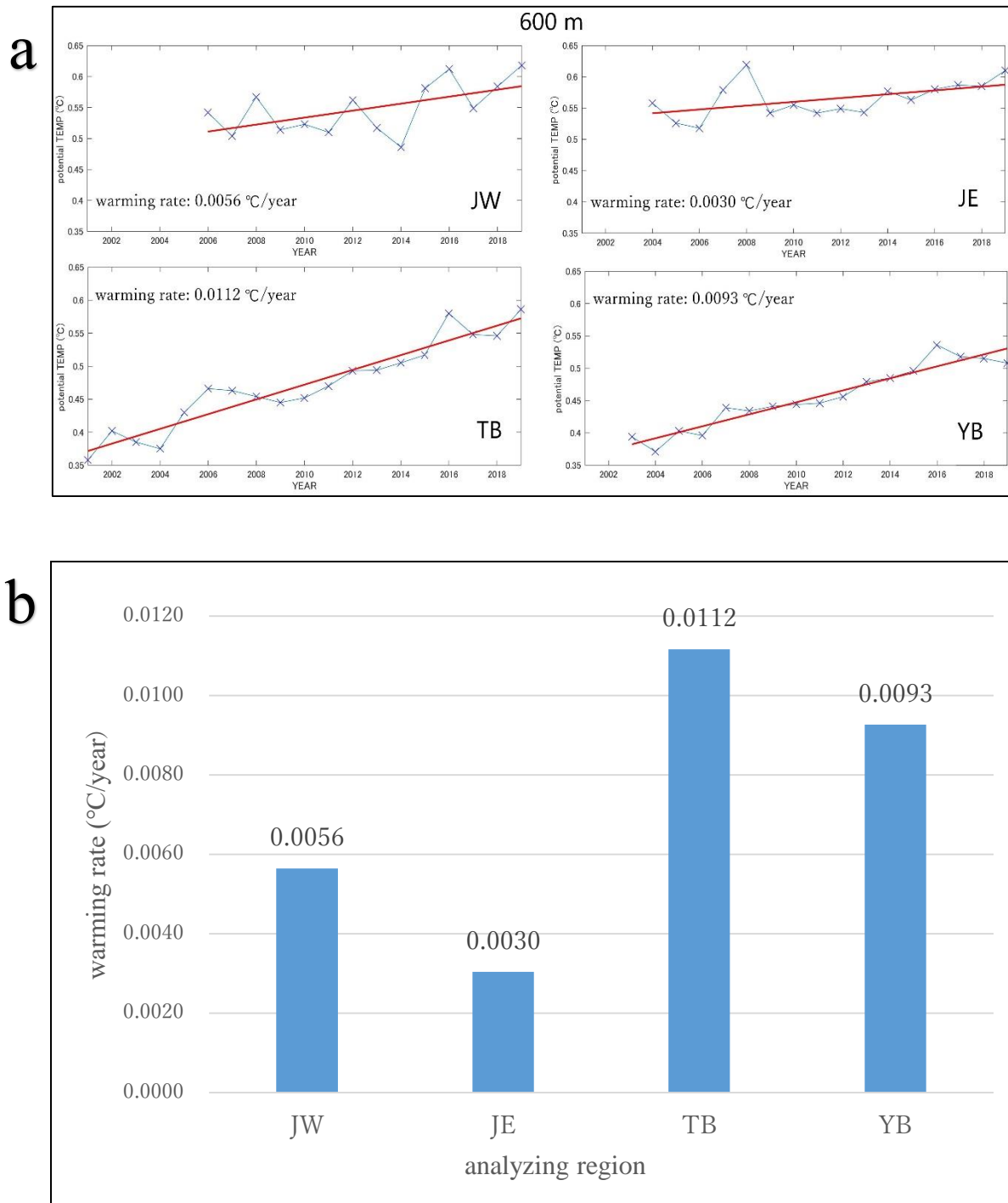


Fig. 3-3 Time-series of potential temperature at 600 m in each region (a). Blue dots denote the annual means and red lines indicate the linear trends. Warming rate of potential temperature in each region at 600 m (b).

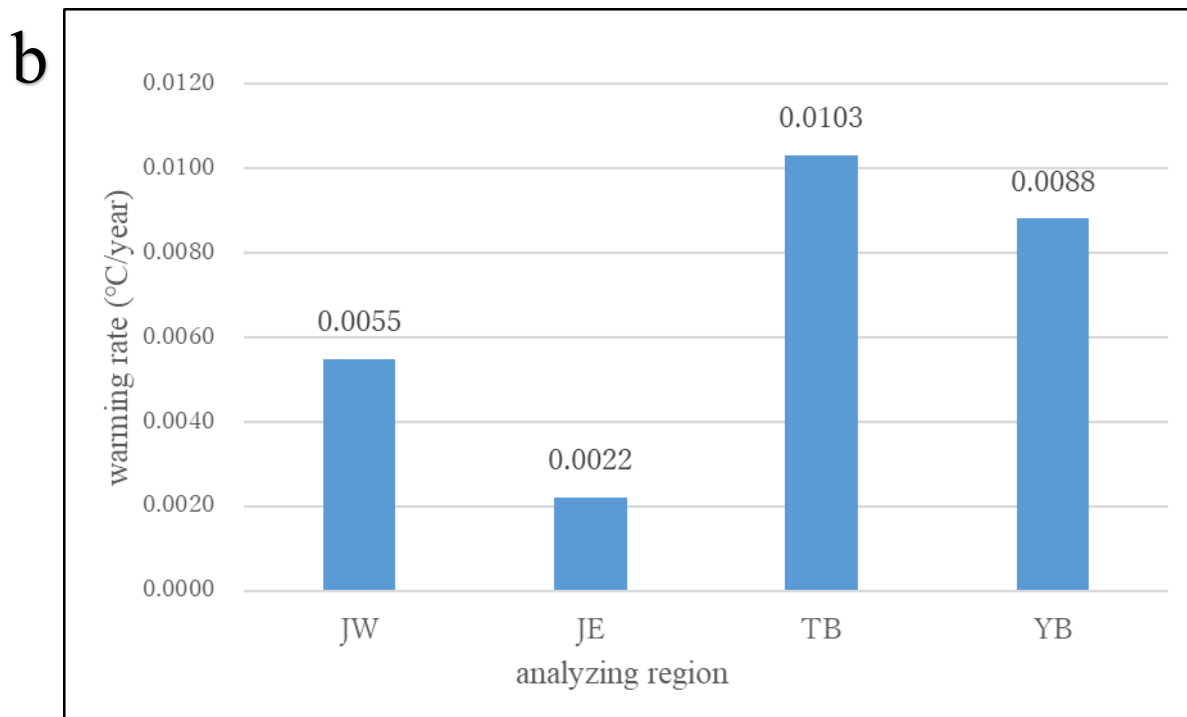
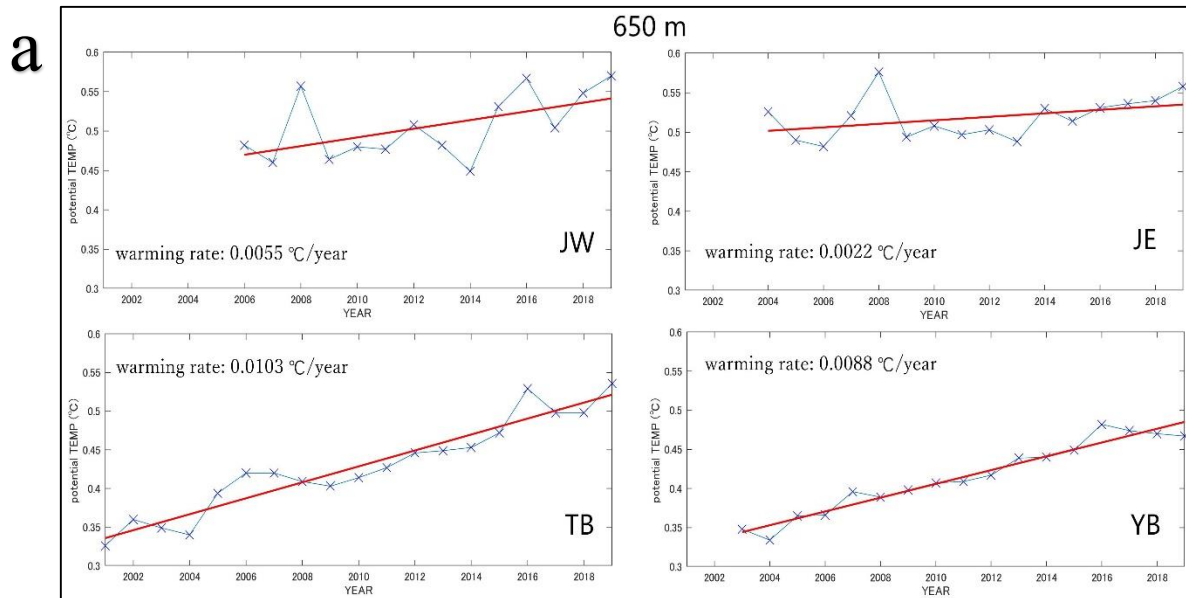


Fig. 3-4 Time-series of potential temperature at 650 m in each region (a). Blue dots denote the annual means and red lines indicate the linear trends. Warming rate of potential temperature in each region at 650 m (b).

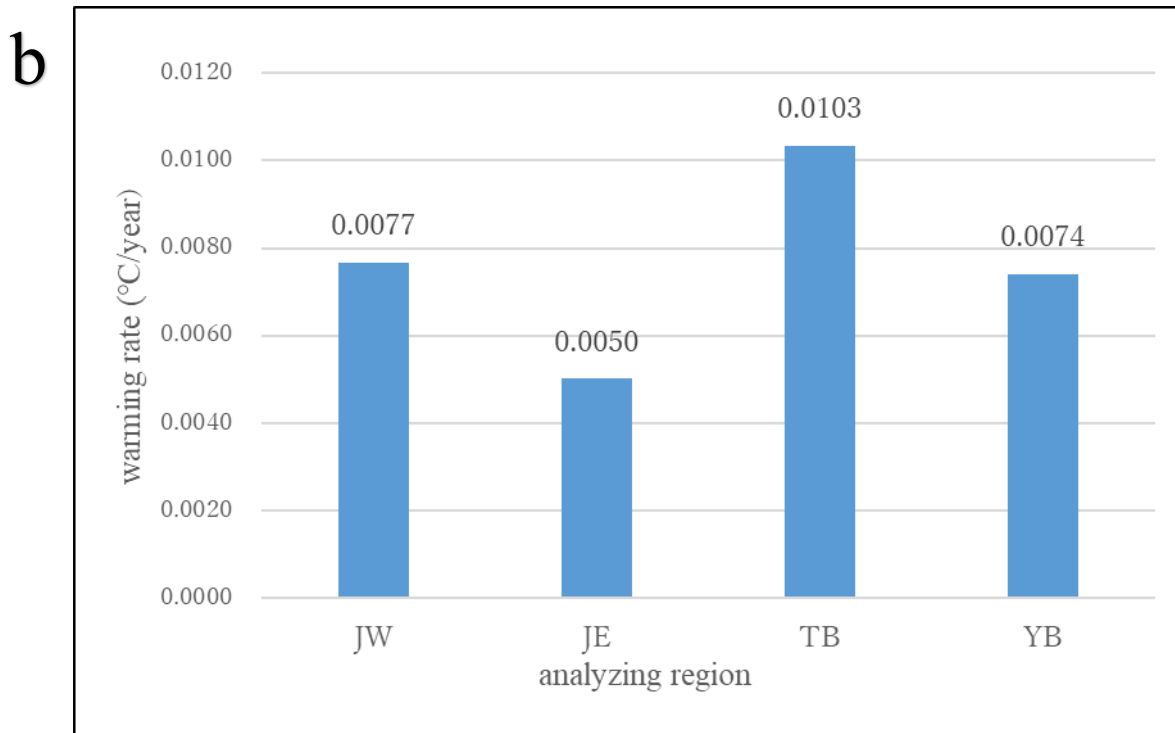
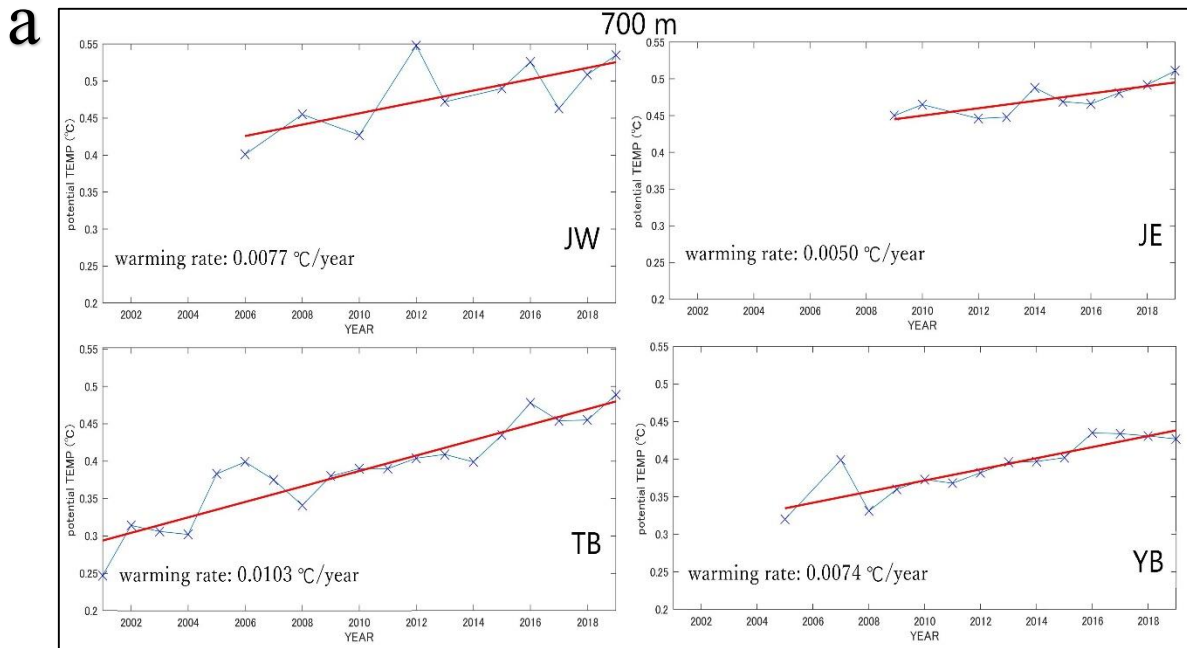


Fig. 3-5 Time-series of potential temperature at 700 m in each region (a). Blue dots denote the annual means and red lines indicate the linear trends. Warming rate of potential temperature in each region at 700 m (b).

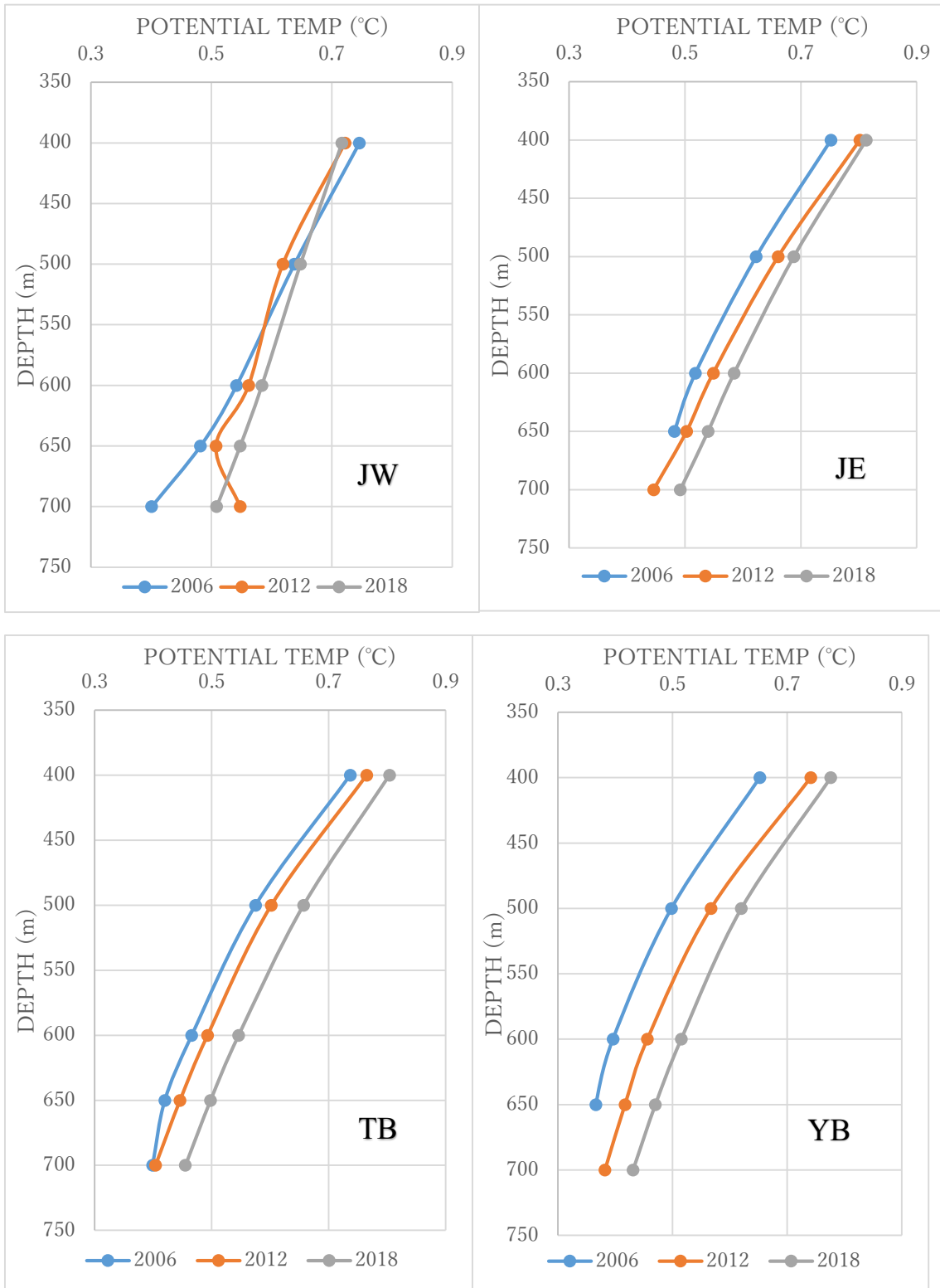


Fig. 3-6 Time-series of potential temperature profiles in JW (upper left), JE (upper right), TB (lower left) and YB (lower right) in 2006, 2012 and 2018.

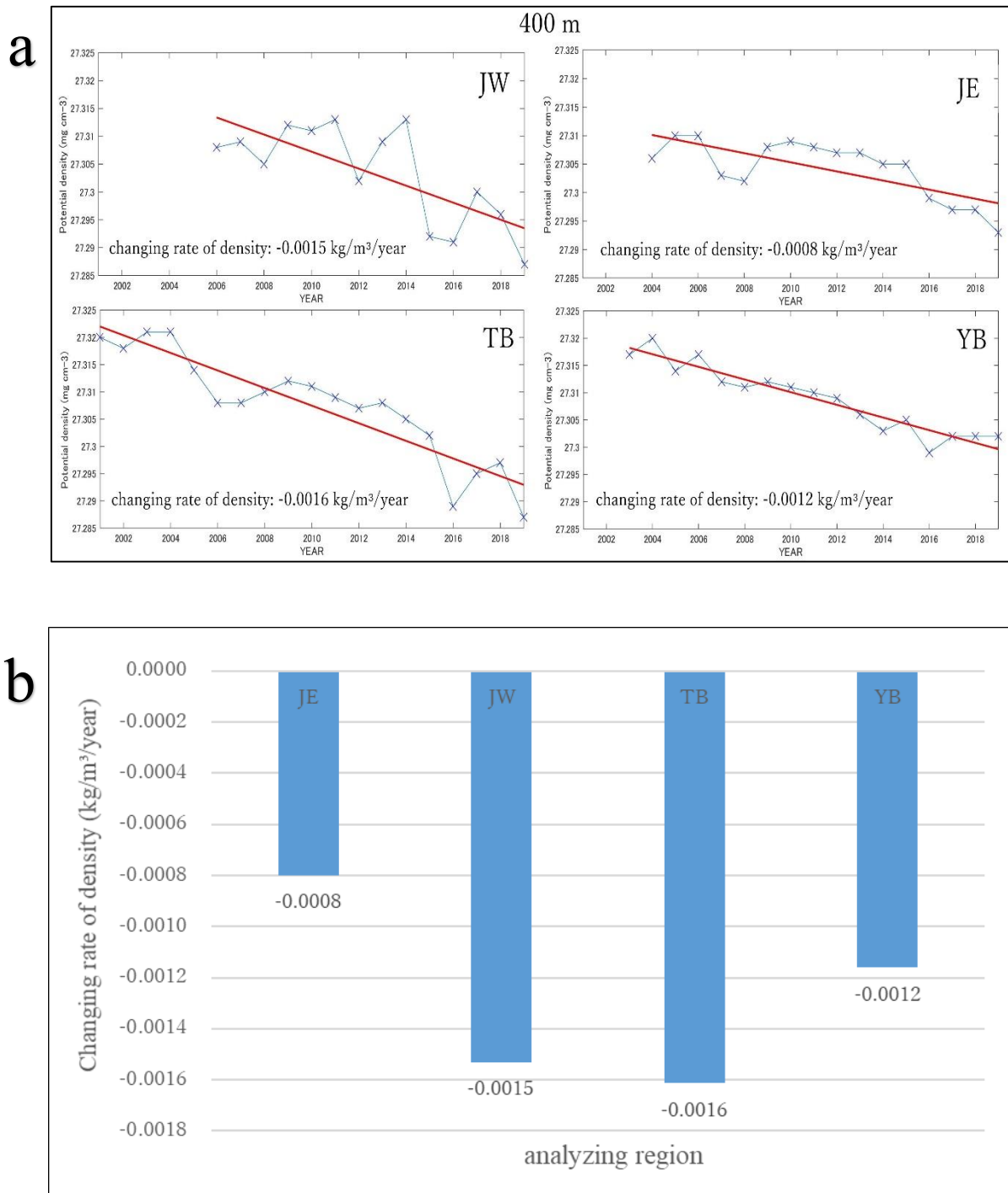


Fig. 3-7 Time-series of potential density at 400 m in each region (a). Blue dots denote the annual means and red lines indicate the linear trends. Changing rate of potential density in each region at 400 m (b).

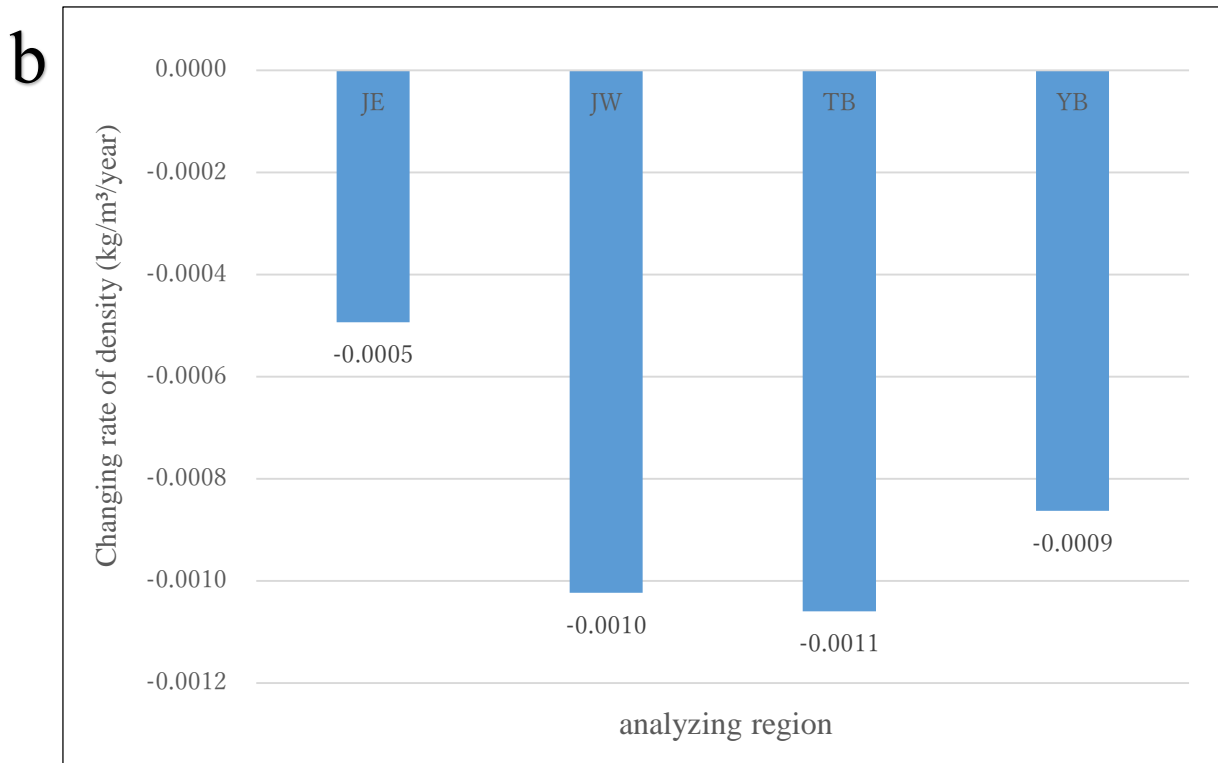
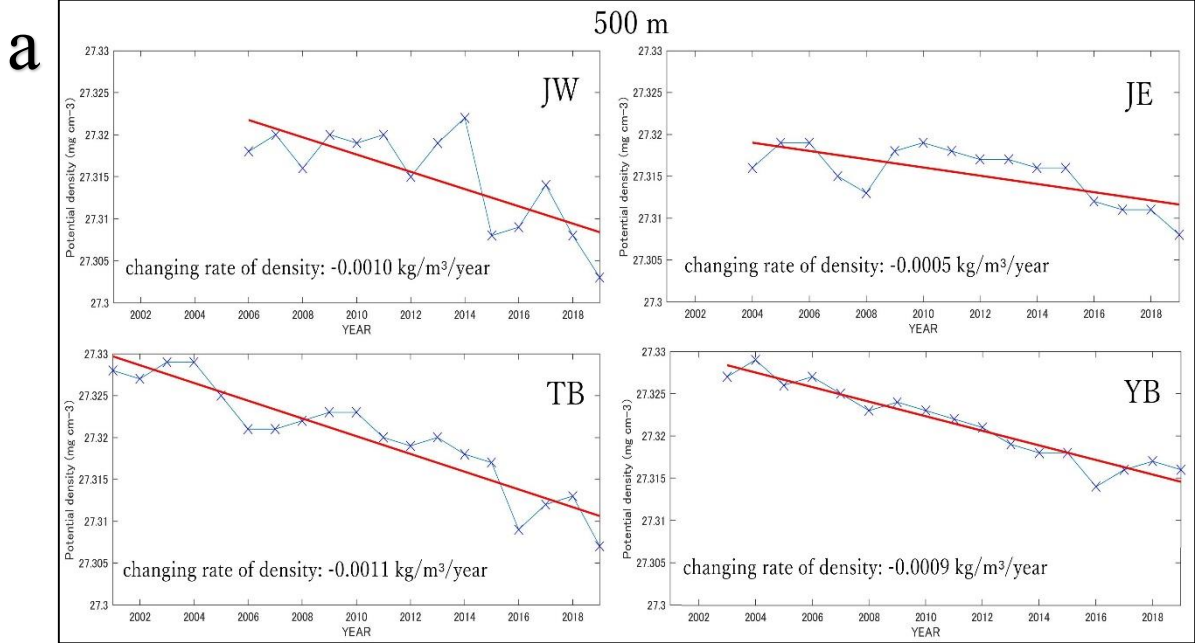


Fig. 3-8 Time-series of potential density at 500 m in each region (a). Blue dots denote the annual means and red lines indicate the linear trends. Changing rate of potential density in each region at 500 m (b).

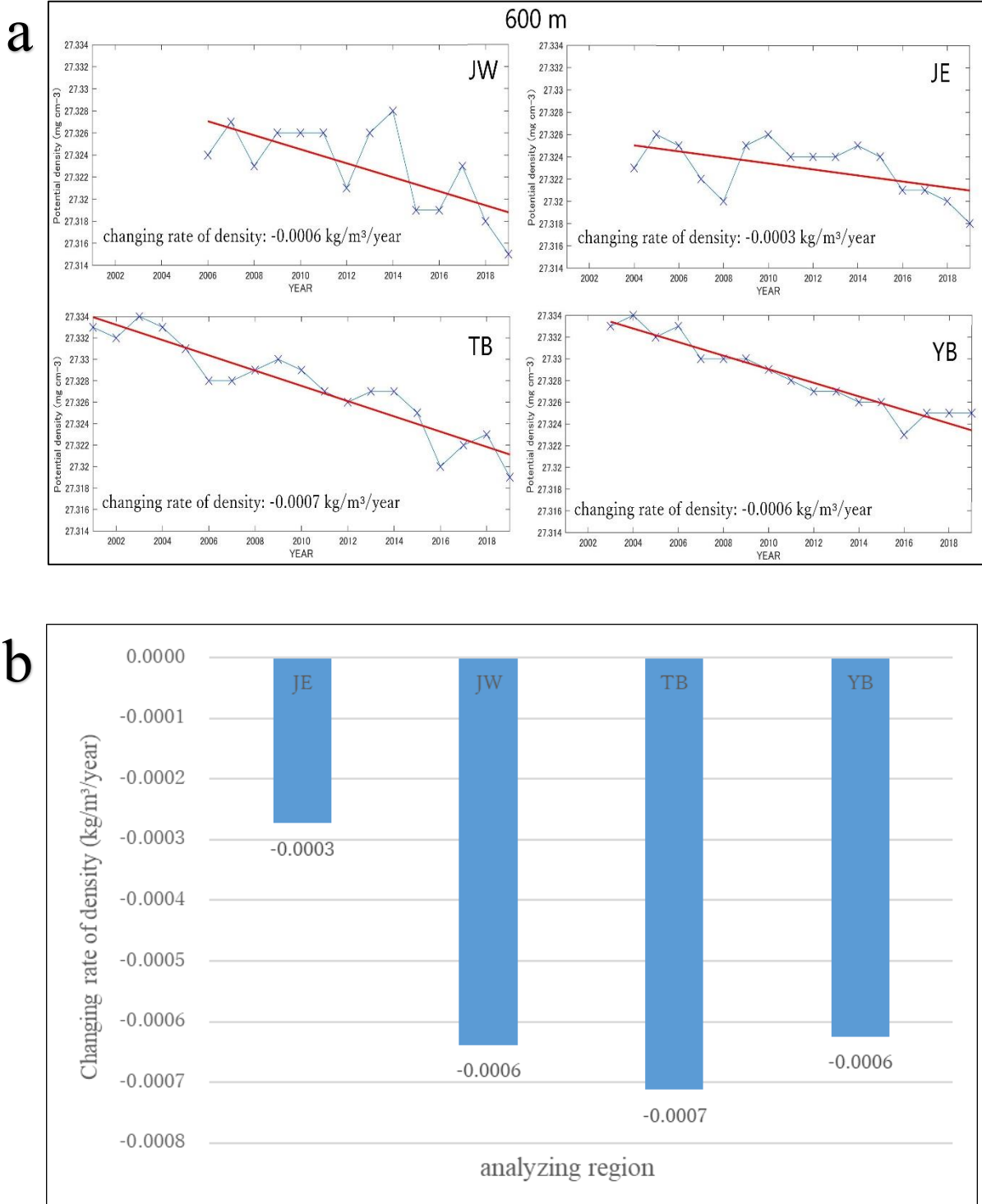


Fig. 3-9 Time-series of potential density at 600 m in each region (a). Blue dots denote the annual means and red lines indicate the linear trends. Changing rate of potential density in each region at 600 m (b).

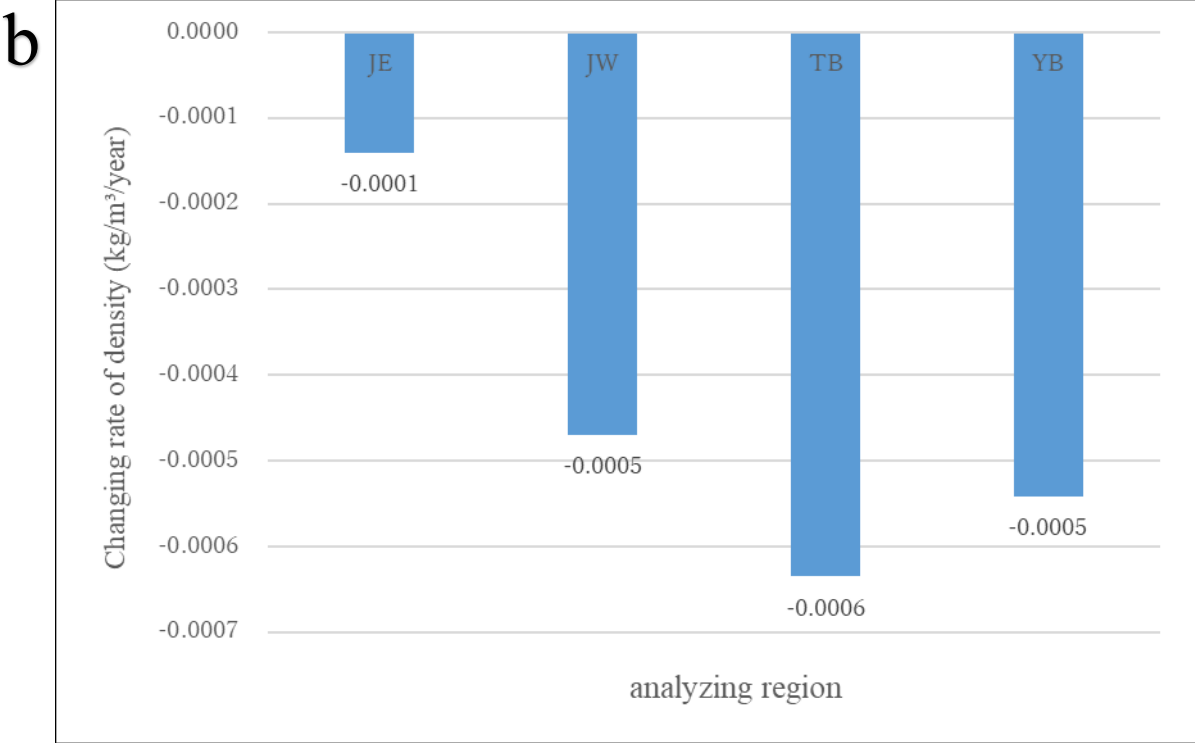
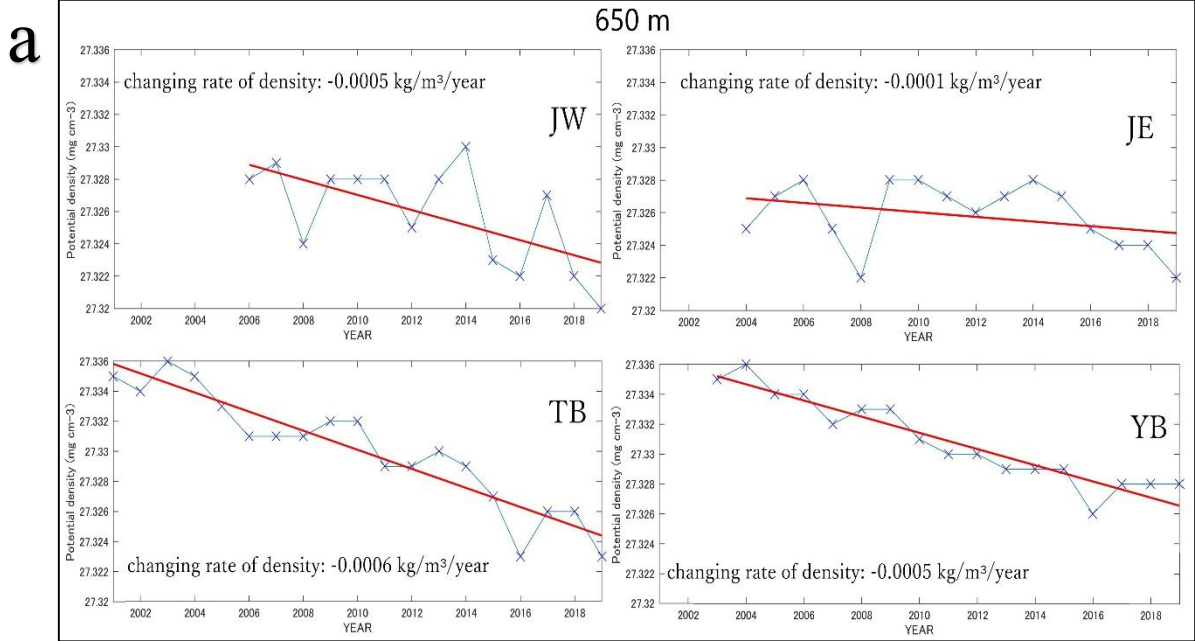
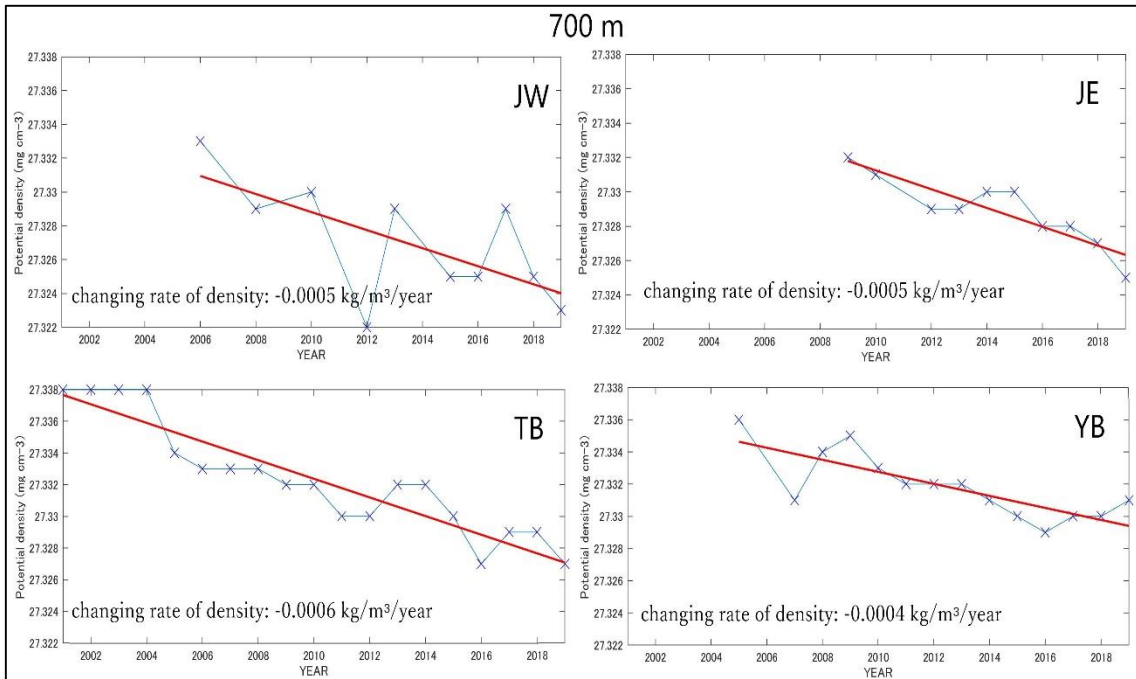


Fig. 3-10 Time-series of potential density at 650 m in each region (a). Blue dots denote the annual means and red lines indicate the linear trends. Changing rate of potential density in each region at 650 m (b).

a



b

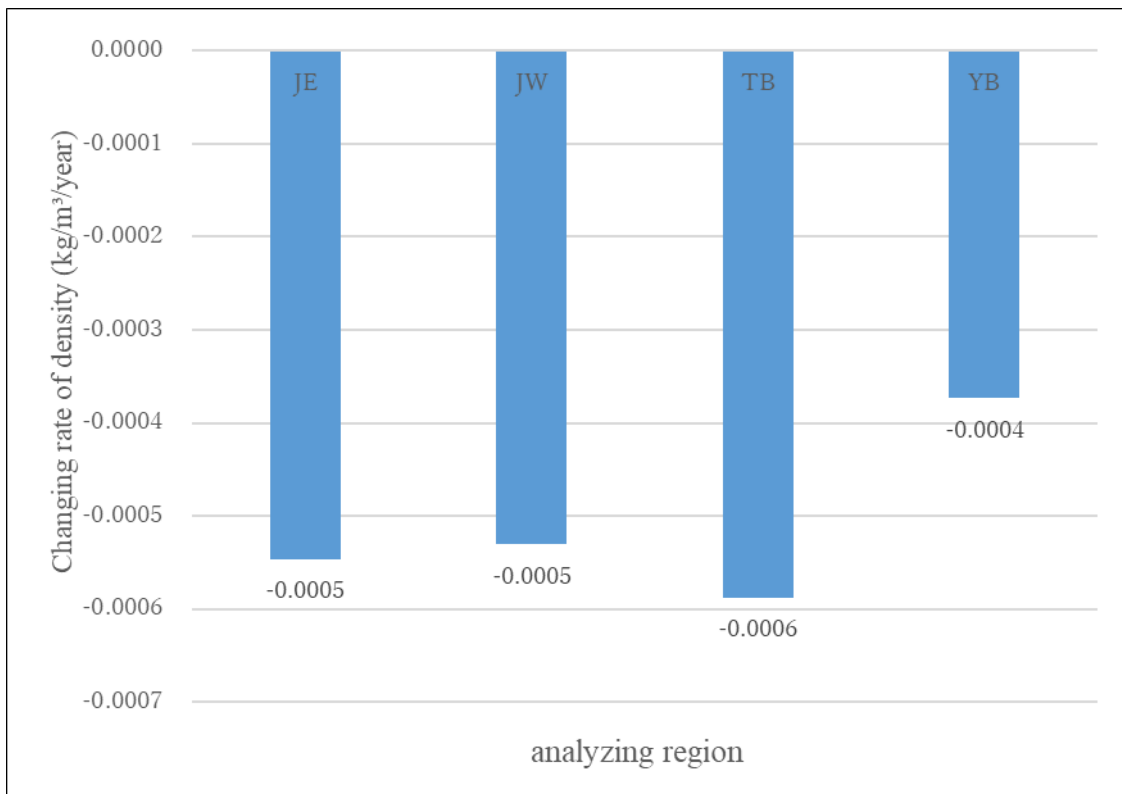


Fig. 3-11 Time-series of potential density at 700 m in each region (a). Blue dots denote the annual means and red lines indicate the linear trends. Changing rate of potential density in each region at 700 m (b).

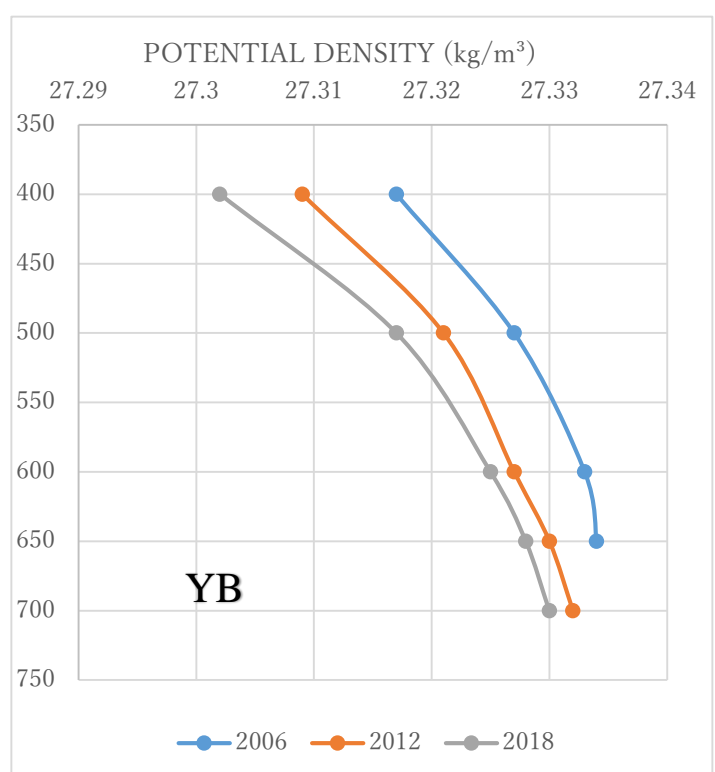
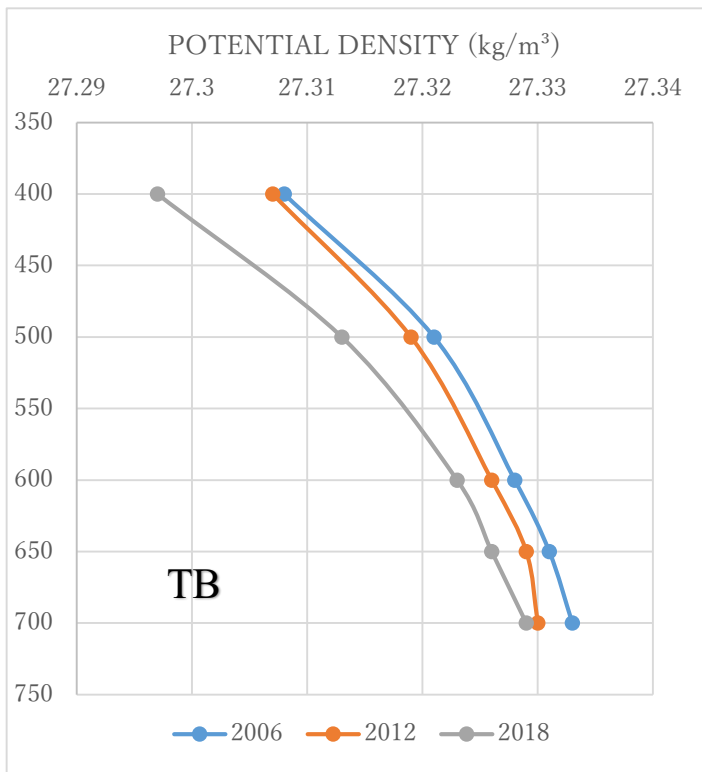
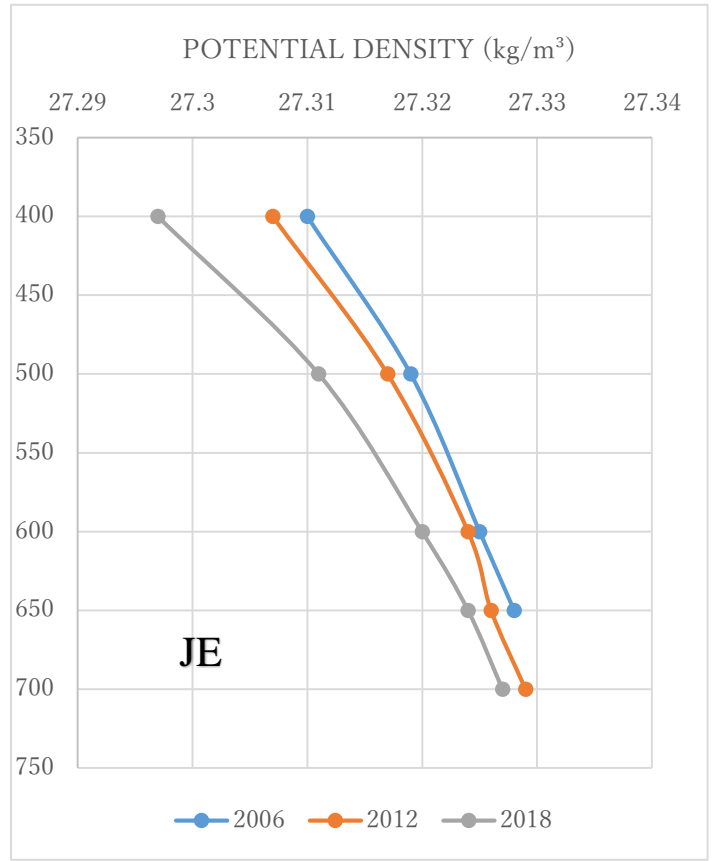
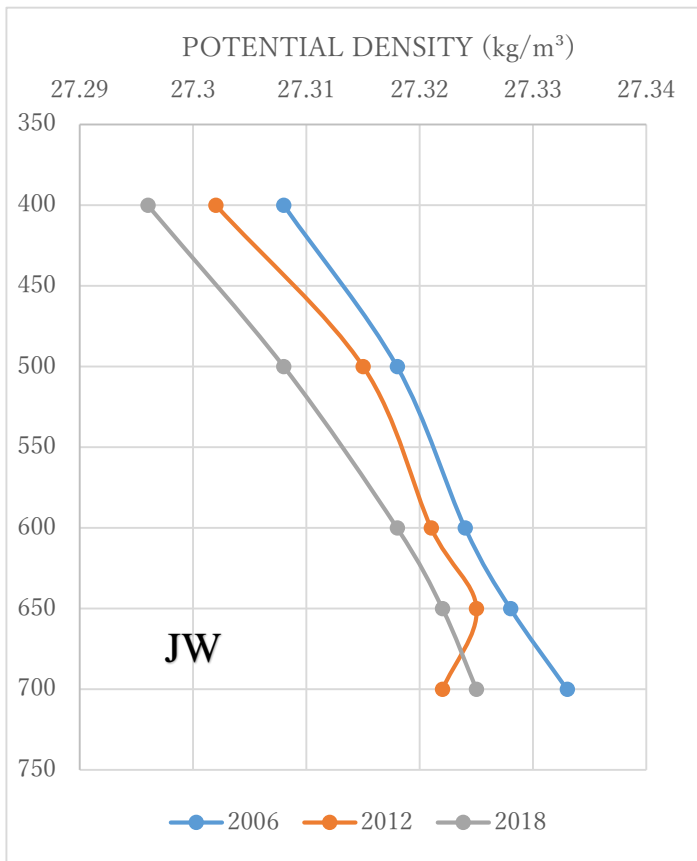


Fig. 3-12 Time-series of potential density profiles in JW (upper left), JE (upper right), TB (lower left) and YB (lower right) in 2006, 2012 and 2018.

4. Discussion

In this study, we showed that the UJSPW is warming in the entire Japan Sea using the Argo floats data. In addition, the warming rates in the southern Japan Sea are higher than those in the northern sea by 2-4 times.

The warming trends in the UJSPW is attributable to global warming. The warming trends in the deep water and bottom waters have been studied by many oceanographers (Gamo 1999, 2011; Minami et al. 1999; Kim et al. 2001), as shown by the warming trends at 2000 m over the recent decades in the Yamato and eastern Japan Basins (Fig. 1-5). Global warming has been suggested as a cause of the warming trends in the deep and bottom waters. Therefore, the warming in the UJSPW is likely to link with that in deeper layer.

Vertical profiles of dissolved oxygen in the Eastern Japan Basin from 1977 to 2010 is shown in Fig. 4-1 (Gamo et al. 2014). It is apparent that dissolved oxygen has decreased year by year. The gradual decrease of dissolved oxygen in the bottom water demonstrates the imbalance between the supply of oxygen from the surface and the oxygen consumption in the bottom water by the decomposition of organic matter falling from the surface. The latter process apparently has exceeded the former one since 1977. From these observational results, following scenario has been presented. In the past, successive cold winters frequently caused the development of deep convection that reached down to the bottom layer, and a large volume of bottom water was produced via this process every year in the region of the JSPW formation. However, since at least the 1970s, with moderate winters accompanied by global warming, deep convection has reduced and the formation of the JSPW have stagnated (Gamo 2011).

The deep circulation deduced from direct current measurements is show in Fig. 4-

2 (Senjyu et al. 2005). The newly formed cold JSPW is transported by the deep circulation from the formation area near Vladivostok to the entire Japan Sea (Fig. 4-2a). The Japan Basin including the JSPW formation area is directly supplied with the cold newly formed JSPW. However, considering the recent stagnation in the JSPW formation, the transport of the new JSPW to the Tsushima and Yamato Basins which are far from the JSPW formation area is likely limited (Fig. 4-2b). As a result, TB and YB in the southern Japan Sea show higher warming rates than JW and JE in the northern sea. This suggests the weakening of deep circulation in the Japan Sea.

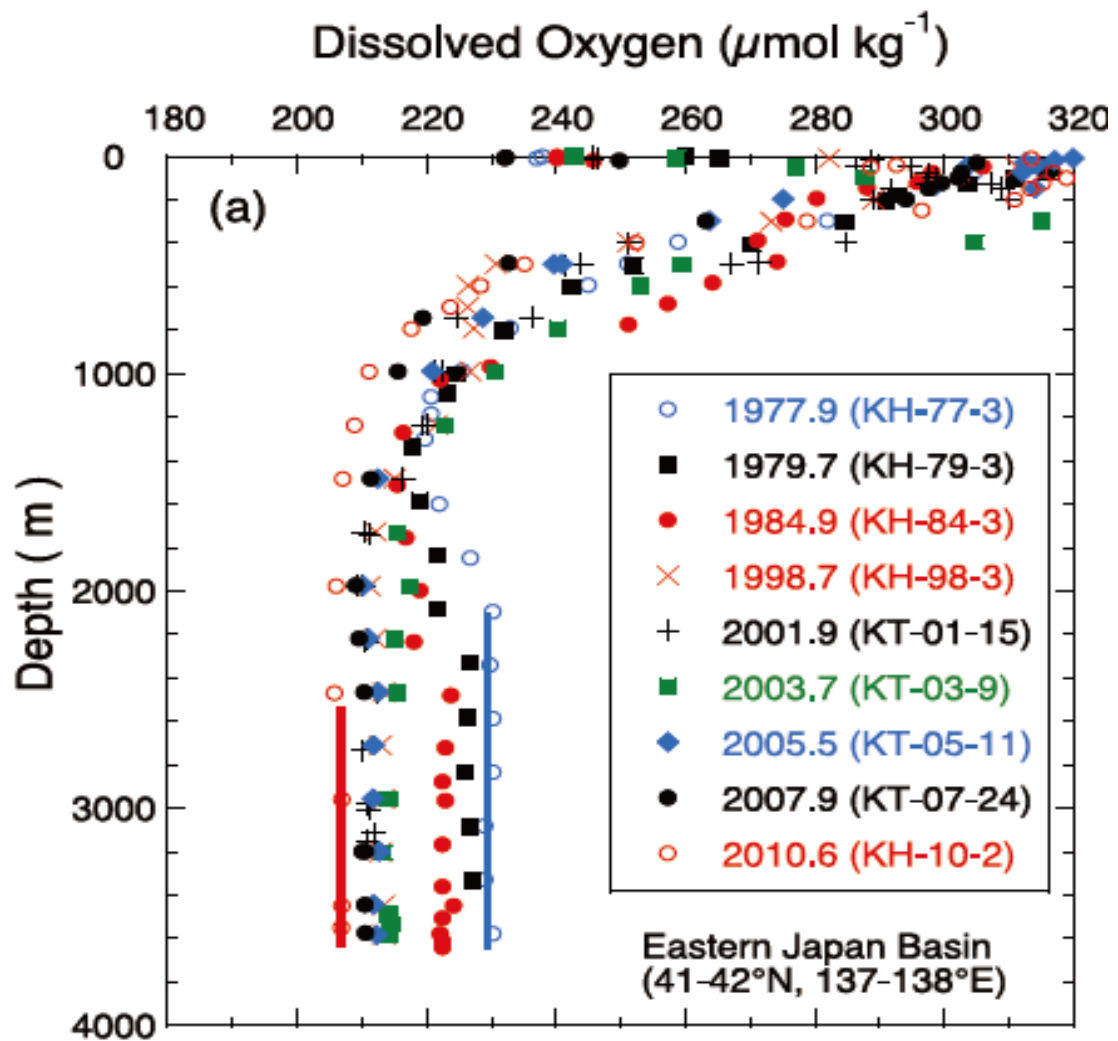


Fig. 4-1 Vertical profiles of dissolved oxygen in the Eastern Japan Basin from 1977 to 2010 (Gamo et al. 2014).

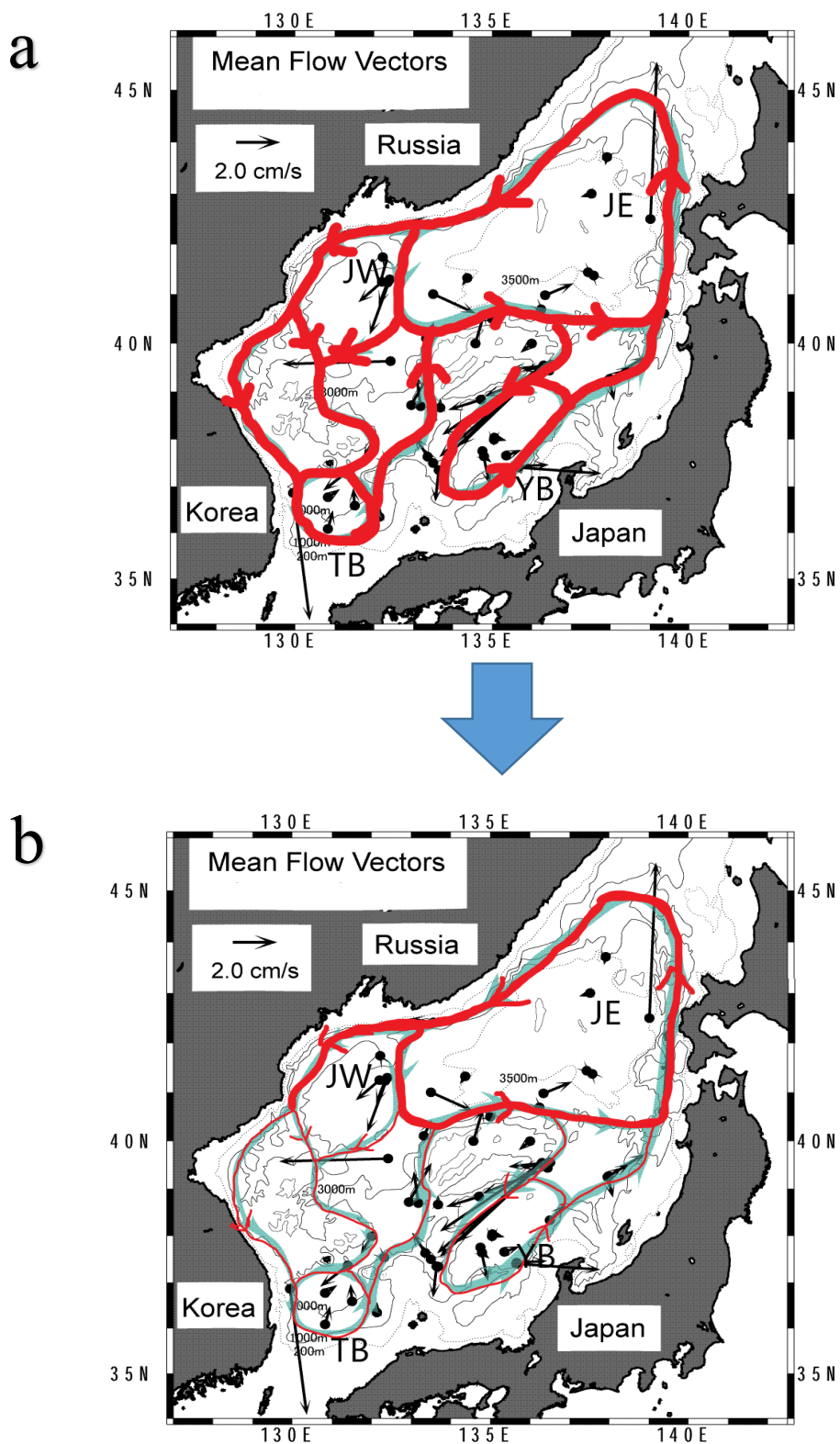


Fig. 4-2 Conceptual view of the Japan Sea deep circulation (Senjyu et al. 2005). (a) the past and (b) present. Thick and thin red lines indicate large and small transport of newly formed JSPW, respectively.

5. Conclusions

The Argo float data were analyzed to investigate the long-term warming trends in the upper portion of the Japan Sea Proper Water during 2001-2019. We obtained the following results:

1. Warming trends in the UJSPW were detected in the entire Japan Sea area. Correspondingly, potential density of UJSPW showed decrease trends in the whole Japan Sea area.
2. The warming rates in TB and YB in the southern Japan Sea were higher than those in JW and JE in the northern sea by 2-4 times in all the analyzed depths.
3. The warming trends in the upper portion of the Japan Sea are attributable to global warming.
4. Inhomogeneous warming rates between the northern and the southern Japan Sea suggest decreasing of newly formed JSPW and the weakening of deep circulation in the Japan Sea.

To confirm above speculation, it is necessary to investigate the difference of warming rates between the northern and the southern Japan Sea in the past.

6. References

- Akima H (1970) A new method of interpolation and smooth curve fitting based on local procedures. *J Assoc Comp Mach* 4:589-602.
- Gamo T (1999) Global warming may have slowed down the deep conveyor belt of a marginal sea of the northwestern Pacific: Japan Sea. *Geophys Res Lett* 26:3137-3140.
- Gamo T (2011) Dissolved oxygen in the bottom water of the Sea of Japan as a sensitive alarm for global climate change. *TrAC Trends Anal Chem* 30:308-1319.
- Gamo T, Nakayama N, Takahata N, Sano Y, Zhang J, Yamazaki E, Taniyasu S, Yamashita N (2014) The Sea of Japan and its unique chemistry revealed by time-series observations over the last 30 years. *Monogr Environ Earth Planets* 2:1-22.
- Kawamura H and Wu P (1998) Formation mechanism of Japan Sea Proper Water in the flux center off Vladivostok. *J Geophys Res* 103:21611-21622.
- Kim K, Kim KR, Min DH, Vlokov Y, Yoon JH, Takematsu M (2001) Warming and structural changes in the east (Japan) Sea: a clue to future changes in global oceans? *Geophys Res Lett* 28:3293-3296.
- Minami H, Kano Y, Ogawa K (1999) Long-term variations of potential temperature and dissolved oxygen of the Japan Sea Proper Water. *J. Oceanogr* 55:197-205.
- Senjyu T (2020) Long-Term Changes in the Abyssal Japan Sea (East Sea): A Physical View. In *Changing Asia-Pacific Marginal Seas, Atmosphere, Earth, Ocean & Space* Springer Nature Singapore Pte Ltd 69-85.
- Senjyu T, Shin HR, Yoon JH, Nagano Z, An HS, Byun SK, Lee CK (2005) Deep flow field in the Japan/East Sea as deduced from direct current measurements. *Deep-Sea Res II* 52:1726-1741.
- Senjyu T and Sudo H (1993) Water characteristics and circulation of the upper portion of

- the Japan Sea Proper Water. *J Mar Sys* 4:349-362.
- Senjyu T and Sudo H (1994) The upper portion of the Japan Sea Proper Water; its source and circulation as deduced from isopycnal analysis. *J Oceanogr* 50:666-690.
- Senjyu T and Sudo H (1996) Interannual variation of the upper portion of the Japan Sea Proper Water and its probable cause. *J Oceanogr* 52:27-42.
- Sudo H (1986) A note on the Japan Sea Proper Water. *Prog Oceanogr* 17: 313-336.
- Uda M (1934) The results of simultaneous oceanographical investigations in the Japan Sea and its adjacent waters in May and June. *J Imp Fish Exp Sta* 5:57-190.
- Yasui M, Yasuoka T, Tanioka K, Shiota O (1967) Oceanographic studies of the Japan Sea (1)-Water characteristics. *Oceanogr Mag* 19:177-192.
- Yoshikawa Y, Awaji T, Akitomo K (1999) Formation and circulation processes of Intermediate Water in the Japan Sea. *J Oceanogr* 29:1701-1722.

7. Acknowledgements

In the course of this study, I have received much guidance, help and support from many people. Here, I would like to extend my sincere gratitude.

First of all, I am greatly indebted to my supervisor, Associate Professor Tomoharu Senjyu from the Research Institute for Applied Mechanics of Kyushu University. He has given me enlightening guidance and valuable suggestions in the whole study process. Without his great patience and constant encouragement, the accomplishment of this thesis would not have been possible. I am also deeply impressed by his strong sense of responsibility and professionalism dedication, which has not only taught me how to do academic research but also set a good example for my future work.

Secondly, I am very indebted to Associate Professor Takahiro Endoh, Project Professor Takeshi Matsuno, Ms. Yurika Yoshikawa, Secretary Naomi Furumoto, and Akie Sakai from the same laboratory for their help during my graduate studies.

Finally, I would like to give my special thanks to my beloved parents and girlfriend. They have given me huge support in the process of studying abroad in terms of economy and convenience of life. Without their support, I cannot study in Japan with peace of mind.